manual muscle test), but no facial muscle weakness. She also showed a waddling gait and decreased deep tendon reflexes. Serum creatine kinase was mildly elevated (385 IU/L; normal, <200 IU/L).

Histochemical and Immunohistochemical Analyses

Muscle tissue from the patient's vastus lateralis muscle showed marked variation in fiber size, scattered fibers with internally placed nuclei, and small angular fibers. There were scattered fibers with rimmed vacuoles (Fig. 2A). No obvious protein aggregates were seen. The intermyofibrillar networks were disorganized (Fig. 2B). Myosin ATPase staining showed an increase in the percentage of type 2C fibers (7%).

By immunohistochemistry, strongly immunoreactive aggregates of myotilin, αB-crystallin, ZASP, desmin (Figs. 2C–F), and actin (data not shown) were observed in a few fibers. Immunohistochemical and immunoblotting studies excluded other diagnosable causes of LGMD.

Immunoblotting Analysis of Myotilin

The patient's muscle specimen showed an increased intensity of the 57-kd band corresponding to the amount of myotilin monomers compared with the band intensity in a control sample. On the other hand, the 110-kd band corresponding to myotilin dimer was fainter in the patient's sample than in the control muscle (Fig. 2G).

Y2H Analysis for the MYOT Mutation

To determine the effect of the p.R405K mutation on protein-protein interactions, we used a Y2H system. We first tested the homodimerization capacity of wild and mutant myotilin. We generated *GAL4* DNA-binding domain or activation domain constructs containing wtMYOT or mMYOT and cotransformed them to yeast. All MYOT double transformants grew on low-stringency plates, indicating that no MYOT constructs were intrinsically lethal to the yeast cells. Only wtMYOT double transformant grew on medium- and high-stringency plates; the wtMYOT and mMYOT transformant and the mMYOT double transformant did not grow. These results indicate defective dimerization of mutant myotilin with both wild-type and mutant myotilin.

We next tested the interaction between myotilin and its known binding protein partners ACTA1, ACTN2, and FLNC. We cotransformed yeast with wtMYOT or mMYOT with each of ACTA1, ACTN2, and FLNC. The wtMYOT and ACTA1, mMYOT and ACTA1, wtMYOT and ACTN2, and wtMYOT

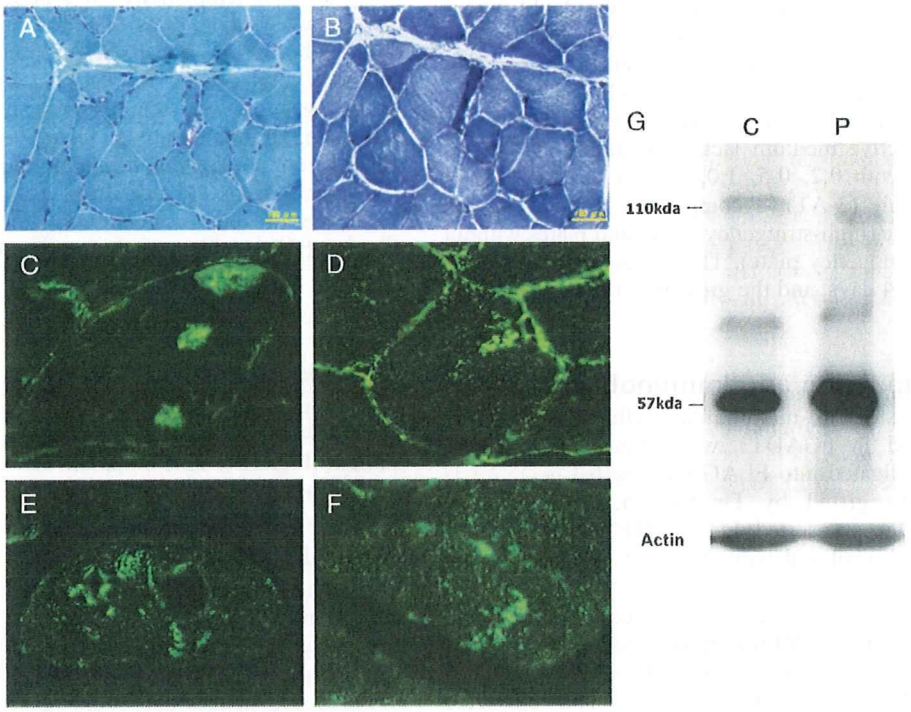

FIGURE 2. Histopathology and immunoblot of muscle from patient with p.R405K mutation. **(A)** Modified Gomori trichrome stain shows scattered fibers with rimmed vacuoles. **(B)** Nicotinamide adenine dinucleotide dehydrogenase–tetrazolium reductase stain shows myofibrillar disorganization. **(C–F)** Immunostaining reveals abnormal accumulation of myotilin **(C)**, desmin **(D)**, Z band alternatively spliced PDZ motif protein **(E)**, and αB-crystallin **(F)**. **(G)** Immunoblot analysis of myotilin in muscle from the patient shows an increased intensity of the 57-kd band that corresponds to monomeric myotilin and a decrease in intensity of the 110-kd band that corresponds to myotilin dimer compared with the control muscle sample. Scale bars = **(A, B)** 100 μm; **(C–F)** 20 μm. C, control; P, patient.

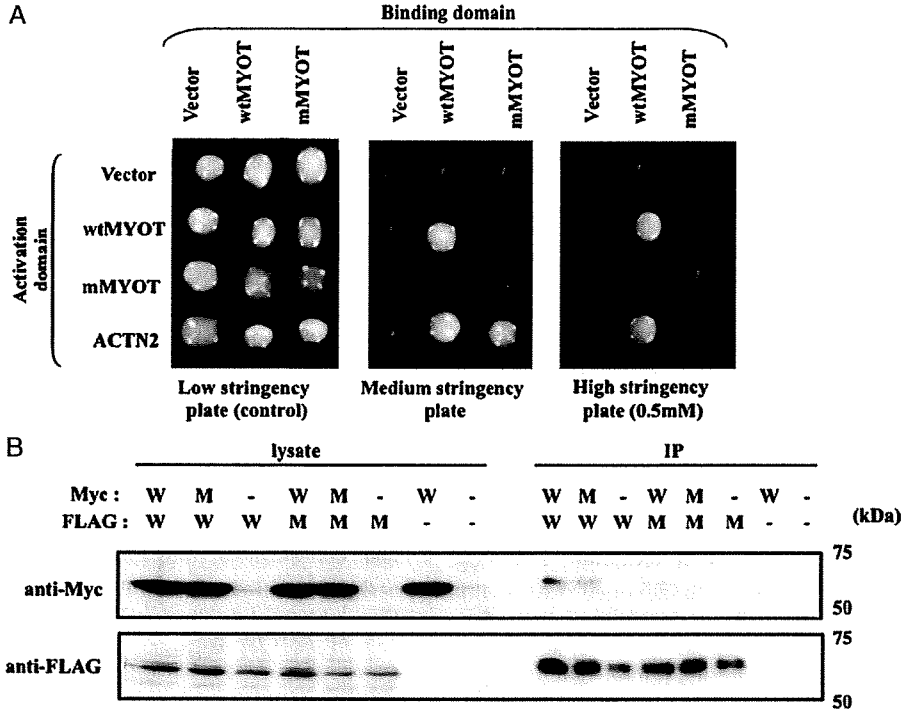

FIGURE 3. Defective homodimerization of mutant myotilin. **(A)** Yeast cells were cotransformed with expression plasmids containing Gal4 DNA-binding or activation domains alone (vector) or fused in frame to full-length human wild-type myotilin (wtMYOT), mutant myotilin (mMYOT), or α-actinin (ACTN2). Double transformants were first selected on low-stringency plates (used as control) and then spotted onto medium- and high-stringency plates. There is a lack of growth of cells coexpressing mMYOT and the corresponding constructs containing mMYOT and wtMYOT on medium- and high-stringency plates (0.5 mmol/L 3-amino-1,2,4-triazole [3-AT]). Cells cotransformed with mMYOT and ACTN2 did not grow on high-stringency plates (0.5 mmol/L 3-AT). **(B)** Myc-tagged myotilin and FLAG-tagged myotilin were coexpressed in COS-7 cells. The cell lysates were subjected to immunoprecipitation with an anti-FLAG M2 affinity gel. The immunoprecipitates (IP) were detected with anti-Myc (upper) or anti-FLAG (lower) antibodies. The mMYOT shows reduced interaction with both wild-type (W) and mutant (M) myotilin. −, empty vector transfected as a control.

and FLNC transformants grew on medium- and high-stringency plates (0.2–2 mmol/L 3-AT). By contrast, mMYOT and ACTN2 transformants grew on medium-stringency and high-stringency plates with 0.2 mmol/L 3-AT but did not grow on high-stringency plates with 0.5, 1, or 2 mmol/L 3-AT (Fig. 3A). This result indicates a decreased binding ability of mutant myotilin to α-actinin. In addition, mMYOT and FLNC transformants did not grow on medium- or high-stringency medium, but FLNC and mMYOT transformants grew on high-stringency medium when Gal4 DNA-binding domain construct containing FLNC was used as the bait (data not shown).

Immunoprecipitation Analysis of Homodimerization

We next used coimmunoprecipitation analysis to confirm the homodimerization defect of mutant myotilin. Myc-tagged wild-type myotilin (Myc-wtMYOT) coimmunoprecipitated with FLAG-tagged wild-type myotilin (FLAG-wtMYOT); this indicates that wild-type myotilin forms a homodimer. On the other hand, other combinations of FLAG-wtMYOT and Myc-tagged mutant myotilin (Myc-mMYOT), FLAG- mMYOT and Myc-wtMYOT, and FLAG-mMYOT and Myc-mMYOT showed decreased interaction (Fig. 3B). These results suggest that the p.R405K mutation in the second immunoglobulin-like domain of myotilin can affect the homodimerization ability of myotilin protein.

DISCUSSION

Limb girdle muscular dystrophy type 1A is an autosomal-dominant muscular dystrophy characterized by progressive proximal muscle weakness and wasting. Distal muscle weakness may occur later (12, 13). The *MYOT* mutations are known to cause LGMD1A, but only a few genetically confirmed LGMD1A patients have been reported to date. Here, we report the first *MYOT* mutation in the Japanese population. The patient had a clinical severity similar to that in other reported LGMD1A patients, and there was also disorganization of myofibrils and rimmed vacuoles in the muscle biopsy tissue. Immunohistochemical analysis revealed accumulation of Z disk proteins (i.e. myotilin, αB-crystallin, ZASP, desmin, and actin) as seen in MFM, thus highlighting the similarities in the pathology of LGMD1A and MFM (21).

Myotilin has 2 immunoglobulin domains in the C terminus of the molecule. Several cytoskeletal proteins have been shown to contain immunoglobulin domains, and most of these proteins are specifically expressed in striated muscle, suggesting a special function for the immunoglobulin domains in this tissue (13, 22). Immunoglobulin domains are known to mediate protein-protein interactions and to serve as dimerization sites and regulators for molecular elasticity and act as modular "spacers" that place an interacting module in the correct position for performing its function (1, 7, 22, 23). The functional importance of the immunoglobulin domains in myotilin was demonstrated by introducing myotilin with mutant immunoglobulin domains in yeast cells that do not express endogenous myotilin (5); these immunoglobulin domains are the site for homodimerization necessary for the actin bundling (8). Our data indicate that the immunoglobulin domains in the C terminus are responsible for the actin binding and bundling ability of myotilin (Fig. 3B).

All previously reported disease-related mutations in *MYOT* are located in the serine-rich amino-terminus of myotilin. The novel p.R405K mutation we identified is located in the second immunoglobulin domain of myotilin, which is important for homodimeric formation and interaction with other proteins (Fig. 1A) (1, 5, 6); this region is highly conserved in vertebrate species, including the mutated residue (Fig. 1B). We found that the 110-kd myotilin dimer band was faint in the patient's muscle sample by immunoblotting, although, as in a previous report (24), the amount of myotilin in the patient's muscle sample was increased. Furthermore, the decreased homodimerization ability of mutant (p.R405K) myotilin was confirmed by the Y2H and immunoprecipitation studies in which interactions of mutant myotilin with both wild-type and mutant myotilin were greatly reduced (Figs. 3A, B). These results suggest that the disturbance of homodimerization caused by the mutated allele may affect the actin-bundling ability of myotilin at the Z disks, resulting in decreased filament stability and gradual disruption in the Z disk in vivo.

Myotilin interacts with 2 important actin-bundling (cross-linker) proteins (i.e. α-actinin and FLNC), forming a complex of 3 actin bundlers at the Z disk. Previous experiments have shown that myotilin enhances the binding of α-actinin to actin (8). The decreased binding ability of mutated myotilin to α-actinin we observed suggests that this altered interaction may loosen the complex formed by these actin bundler proteins leading to a decrease in strength and ability of the Z disk to resist mechanical stress during muscle contraction. On the other hand, mutant myotilin showed no apparent defect in interaction with actin but questionable defective interaction with FLNC by Y2H assay; this issue requires further analysis.

Several hypotheses have been proposed regarding the pathogenesis of the previously reported *MYOT* mutations in Exon 2, including the fact that the serine-rich domain contains a hydrophobic stretch that mediates the localization of small amounts of myotilin to the sarcolemmal membrane. *MYOT* mutations may elongate this hydrophobic stretch, possibly disturbing its interactions with the sarcolemmal membrane (12). It has also been suggested that these mutations may disrupt the binding of myotilin with α-actinin, FLNC, or a novel protein-binding partner (12). None of these hypotheses have been proven. Disease-associated substitutions in myotilin did not affect the localization or actin-bundling ability of myotilin, suggesting that the pathogenic mechanism of the myotilin mutations examined may be independent of its actin-modulating effects (5). In contrast to the previously reported mutations (5, 13), ours is the first report to demonstrate a functional abnormality caused by mutated myotilin. Our data suggest that the p.R405K missense mutation disrupts myotilin homodimerization and decreases the interaction between myotilin and α-actinin, which subsequently may affect its actin-bundling ability.

ACKNOWLEDGMENTS

The authors thank Dr O. Carpén (University of Helsinki) for the kind gift of anti-myotilin antibody and Dr S. Ishiura (University of Tokyo) for providing the FLAG-inserted pcDNA3.1 V5/HisA vector. The authors also thank Dr R. Gabor (National Center of Neurology and Psychiatry) for his help in the Y2H assay.

REFERENCES

1. Salmikangas P, Mykkanen OM, Gronholm M, et al. Myotilin, a novel sarcomeric protein with two Ig-like domains, is encoded by a candidate gene for limb-girdle muscular dystrophy. Hum Mol Genet 1999;8:1329–36
2. Parast MM, Otey CA. Characterization of palladin, a novel protein localized to stress fibers and cell adhesions. J Cell Biol 2000;150:643–56
3. Mykkanen OM, Gronholm M, Ronty M, et al. Characterization of human palladin, a microfilament-associated protein. Mol Biol Cell 2001;12:3060–73
4. Bang ML, Mudry RE, McElhinny AS, et al. Myopalladin, a novel 145-kilodalton sarcomeric protein with multiple roles in Z-disc and I-band protein assemblies. J Cell Biol 2001;153:413–27
5. von Nandelstadh P, Gronholm M, Moza M, et al. Actin-organising properties of the muscular dystrophy protein myotilin. Exp Cell Res 2005;310:131–39
6. van der Ven PF, Wiesner S, Salmikangas P, et al. Indications for a novel muscular dystrophy pathway. Gamma-filamin, the muscle-specific filamin isoform, interacts with myotilin. J Cell Biol 2000;151:235–48
7. Gontier Y, Taivainen A, Fontao L, et al. The Z-disc proteins myotilin and FATZ-1 interact with each other and are connected to the sarcolemma via muscle-specific filamins. J Cell Sci 2005;118:3739–49
8. Salmikangas P, van der Ven PF, Lalowski M, et al. Myotilin, the limb-girdle muscular dystrophy 1A (LGMD1A) protein, cross-links actin filaments and controls sarcomere assembly. Hum Mol Genet 2003;12:189–203
9. Selcen D, Engel AG. Mutations in myotilin cause myofibrillar myopathy. Neurology 2004;62:1363–71
10. Foroud T, Pankratz N, Batchman AP, et al. A mutation in myotilin causes spheroid body myopathy. Neurology 2005;65:1936–40
11. Olivé M, Goldfarb LG, Shatunov A, et al. Myotilinopathy: Refining the clinical and myopathological phenotype. Brain 2005;128:2315–26
12. Hauser MA, Conde CB, Kowaljow V, et al. Myotilin mutation found in second pedigree with LGMD1A. Am J Hum Genet 2002;71:1428–32
13. Hauser MA, Horrigan SK, Salmikangas P, et al. Myotilin is mutated in limb girdle muscular dystrophy 1A. Hum Mol Genet 2000;9:2141–47
14. Penisson-Besnier I, Talvinen K, Dumez C, et al. Myotilinopathy in a family with late onset myopathy. Neuromuscul Disord 2006;16:427–31
15. Berciano J, Gallardo E, Dominguez-Perles R, et al. Autosomal dominant distal myopathy with a myotilin S55F mutation: Sorting out the phenotype. J Neurol Neurosurg Psychiatry 2008;79:205–8

16. Schröder R, Reimann J, Salmikangas P, et al. Beyond LGMD1A: Myotilin is a component of central core lesions and nemaline rods. Neuromuscul Disord 2003;13:451–55
17. Matsumoto H, Hayashi YK, Kim DS, et al. Congenital muscular dystrophy with glycosylation defects of alpha-dystroglycan in Japan. Neuromuscul Disord 2005;15:342–48
18. Starcevic M, Dell'Angelica EC. Identification of snapin and three novel proteins (BLOS1, BLOS2, and BLOS3/reduced pigmentation) as subunits of biogenesis of lysosome-related organelles complex-1 (BLOC-1). J Biol Chem 2004;279:28393–401
19. Falcon-Perez JM, Starcevic M, Gautam R, Dell'Angelica EC. BLOC-1, a novel complex containing the pallidin and muted proteins involved in the biogenesis of melanosomes and platelet-dense granules. J Biol Chem 2002;277:28191–99
20. Mitsuhashi H, Futa E, Sasagawa N, et al. Csk-homologous kinase interacts with SHPS-1 and enhances neurite outgrowth of PC12 cells. J Neurochem 2008;105:101–12
21. Selcen D. Myofibrillar myopathies. Curr Opin Neurol 2008;21:585–99
22. Vaughan KT, Weber FE, Einheber S, et al. Molecular cloning of chicken myosin-binding protein (MyBP) H (86-kDa protein) reveals extensive homology with MyBP-C (C-protein) with conserved immunoglobulin C2 and fibronectin type III motifs. J Biol Chem 1993;268:3670–76
23. Fucini P, Renner C, Herberhold C, et al. The repeating segments of the F-actin cross-linking gelation factor (ABP-120) have an immunoglobulin-like fold. Nat Struct Biol 1997;4:223–30
24. Barrachina M, Moreno J, Juves S, et al. Target genes of neuron restrictive silencer factor are abnormally up-regulated in human myotilinopathy. Am J Pathol 2007;171:1312–23

Mitochondrion 9 (2009) 115–122

Contents lists available at ScienceDirect

Mitochondrion

journal homepage: www.elsevier.com/locate/mito

Different effects of novel mtDNA G3242A and G3244A base changes adjacent to a common A3243G mutation in patients with mitochondrial disorders

Masakazu Mimaki [a], Hideyuki Hatakeyama [a], Takashi Ichiyama [b], Hiroshi Isumi [b], Susumu Furukawa [b], Manami Akasaka [c], Atsushi Kamei [c], Hirofumi Komaki [a], Ichizo Nishino [d], Ikuya Nonaka [e], Yu-ichi Goto [a,*]

[a] Department of Mental Retardation and Birth Defect Research, National Institute of Neuroscience, National Center of Neurology and Psychiatry (NCNP), 4-1-1 Ogawahigashi, Kodaira, Tokyo, Japan
[b] Department of Pediatrics, Yamaguchi University School of Medicine, Yamaguchi, Japan
[c] Department of Pediatrics, Iwate Medical University, Iwate, Japan
[d] Department of Neuromuscular Research, National Institute of Neuroscience, NCNP, Kodaira, Tokyo, Japan
[e] National Center Hospital for Mental, Nervous and Muscular Disorders, NCNP, Kodaira, Tokyo, Japan

ARTICLE INFO

Article history:
Received 30 July 2008
Received in revised form 9 November 2008
Accepted 12 January 2009
Available online 21 January 2009

Keywords:
Mitochondrial DNA tRNA$^{Leu(UUR)}$ gene
Mutation
Mitochondrial myopathy encephalopathy lactic acidosis and stroke-like episodes (MELAS)
Cybrid
ATP production
BN-PAGE

ABSTRACT

Two novel mitochondrial DNA base changes were identified at both sides of the 3243A > G mutation, the most common mutation associated with mitochondrial myopathy, encephalopathy, lactic acidosis, and stroke-like episodes (MELAS). One was a 3244G > A transition in a girl with MELAS. The other was a 3242G > A transition in a girl with a mitochondrial disorder without a MELAS phenotype. Although the two base changes were adjacent to the 3243A > G mutation, they had different effects on the clinical phenotype, muscle pathology, and respiratory chain enzyme activity. Investigations of the different effects of the 3244G > A and 3242G > A base changes may provide a better understanding of tRNA dysfunction in mitochondrial disorders.

1. Introduction

Mutations in mitochondrial tRNA genes are the most common molecular causes of mitochondrial encephalomyopathies. In particular, many mutations have been reported in the mitochondrial tRNA$^{Leu(UUR)}$ gene, indicating that the region is a hot spot for mutations (MITOMAP: a Human Mitochondrial Genome Database, http://www.mitomap.org/). Among them, an A-to-G mutation at nucleotide position (np) 3243 was the first reported in the mitochondrial tRNA$^{Leu(UUR)}$ gene (Goto et al., 1990) and is the most prevalent mutation in all ethnicities. This mutation demonstrates defects at several levels. At the molecular level, it causes decreased protein synthesis (Chomyn et al., 1992), transcription termination impairment (Hess et al., 1991), and an anticodon modification abnormality (Yasukawa et al., 2000; Suzuki et al., 2002). At the cellular level, it is associated with heteroplasmy and typical mitochondrial morphological findings, such as ragged-red fibers and strong SDH-reactive blood vessels (Goto et al., 1990; Sakuta and Nonaka, 1989). At the organ level, the mutation is strongly associated with mitochondrial myopathy, encephalopathy, lactic acidosis, and stroke-like episodes (MELAS) (Goto et al., 1990, 1992).

Mutations in the mitochondrial tRNA$^{Leu(UUR)}$ gene demonstrate marked phenotypic variability, ranging from pure myopathy (Campos et al., 2001; Hadjigeorgiou et al., 1999) to MELAS; however, the pathogenicity of only a few mutations including 3243A > G has been confirmed. As new cases of tRNA mutations accumulate and are analyzed, we will develop an understanding of their pathogenesis and the genotype–phenotype relationship.

Here, we report two new cases harboring novel base changes at both sides of the 3243A > G mutation. One was a 3244G > A transition and the other was a 3242G > A transition. We studied these patients clinically, pathologically, biochemically, and genetically to determine the different effects of these novel base changes that are adjacent to the common 3243A > G mutation.

* Corresponding author. Tel.: +81 42 346 1713; fax: +81 42 346 1743.
E-mail address: goto@ncnp.go.jp (Y.-i. Goto).

1567-7249/$ - see front matter © 2009 Elsevier B.V. and Mitochondria Research Society. All rights reserved.
doi:10.1016/j.mito.2009.01.005

2. Materials and methods

2.1. Clinical investigations

2.1.1. Patient 1

Patient 1 was a 6-year-old girl born to nonconsanguinous parents after an uncomplicated pregnancy and birth. Her family history was unremarkable, including that of her mother and sister. At 4 years of age, she had an attack with vomiting followed by loss of consciousness, and clonic convulsions of the right arm. After the first attack, she had recurrent seizures with episodic vomiting and gradually developed psychomotor deterioration. She was unable to run by the age of 6. At that time, she could converse, but often counted incorrectly. Her limbs were atrophic, and her muscle tone and power were reduced. The patient had no cerebellar signs, myoclonus, or abnormalities of the cranial nerves. A laboratory examination revealed elevated lactate and pyruvate levels in the blood (lactate, 4.81 mmol/l; pyruvate, 0.117 mmol/l; normal, 0.44–1.33 and 0.045–0.113, respectively) and in the cerebrospinal fluid (lactate, 13.3 mmol/l; pyruvate, 0.451 mmol/l). Computed tomography (CT) of the brain revealed calcifications of the basal ganglia and diffuse cerebral atrophy (Fig. 1A). Magnetic resonance imaging (MRI) images of the brain showed diffuse abnormal high T2-weighted signals in the cerebral white matter, especially around the lateral ventricles, and multiple patchy T2-weighted signals in the cerebral cortex.

2.1.2. Patient 2

Patient 2 was a female born to nonconsanguinous parents. Her mother was healthy without any neurological symptoms. Her elder sister had a short stature due to Turner's syndrome with a typical 45X karyotype, but had no other symptoms of mitochondrial disorders. A birth weight of 1985 g at 37 weeks of gestation indicated intrauterine growth retardation. At birth, she had difficulty in sucking and became tachypneic and anemic, but she gradually improved and was discharged from the hospital. At 5 months of age, she was admitted to a hospital due to muscle floppiness and failure to thrive. She showed generalized hypotonia with absence of head control. She developed respiratory failure, heart failure, renal failure due to tubular dysfunction, and lactic acidosis, and therefore, she needed artificial ventilation. An echocardiogram indicated hypertrophic and dilatated cardiomyopathy. A laboratory examination revealed elevated lactate and pyruvate levels in the blood (lactate, 11.0 mmol/l; pyruvate, 0.31 mmol/l) and in the cerebrospinal fluid (lactate, 13.0 mmol/l; pyruvate, 0.44 mmol/l). She also had a significantly elevated creatine kinase (616 IU/l; normal, 43–170). CT and MRI images of the brain revealed nonspecific diffuse cerebral atrophy (Fig. 1A). After discharge from the hospital, she received artificial ventilation four times because of severe acidosis due to infection. However, after the age of 2 years, manifestations including acidosis, renal function, cardiac function, and muscle tonus slowly improved and she showed gradual psychomotor development without any deterioration.

Written informed consent was obtained from the parents of these patients to perform a muscle biopsy, molecular analysis, and biochemical studies.

2.2. Histopathological study

A biopsy from the *biceps brachii* muscle was frozen in isopentane chilled with liquid nitrogen, and serial frozen sections were stained with hematoxylin–eosin, modified Gomori trichrome (mGT), succinate dehydrogenase (SDH), cytochrome *c* oxidase (COX) by several histochemical methods.

2.3. Molecular genetic studies

DNA extraction, polymerase chain reaction (PCR), and total mitochondrial DNA (mtDNA) sequencing were performed, as described elsewhere (Akanuma et al., 2000). We applied the long

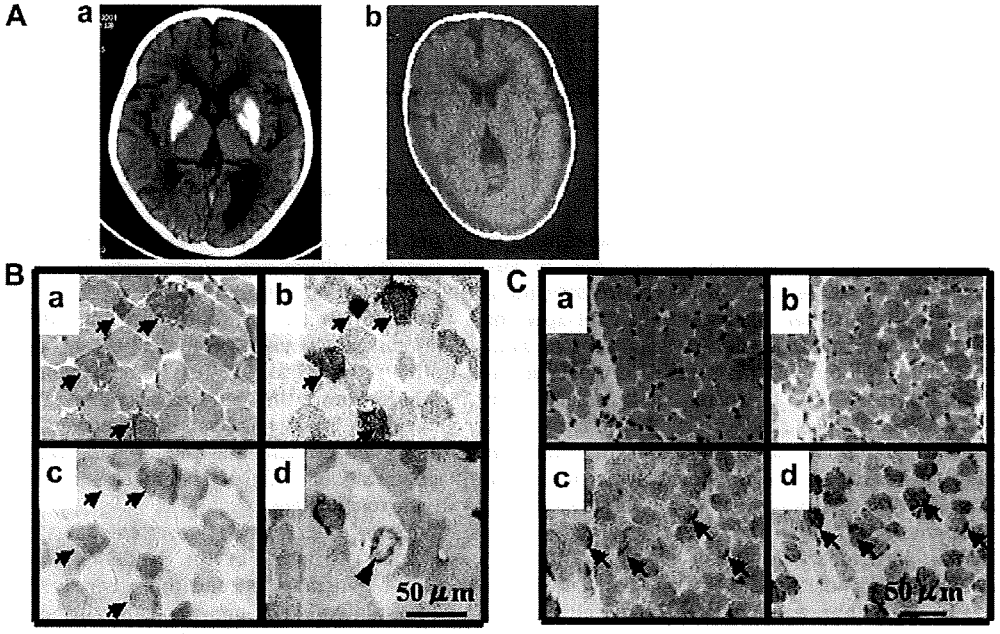

Fig. 1. Computed tomography and histochemical analysis. (A) Computed tomography of the brain of patient 1 (a) revealed calcifications of the basal ganglia and diffuse cerebral atrophy, and of patient 2 (b) revealed mild cerebral atrophy. Morphological analysis of the skeletal muscle of patient 1 (B) and patient 2 (C). In patient 1, ragged-red fibers (RRFs) (arrows) depicted by modified Gomori trichrome (a) and succinate dehydrogenase (SDH) stains. (b) Cytochrome c oxidase (COX) stain (c) revealed a focal COX deficiency, but most of the RRFs reflected intact COX activity (arrows). A strongly SDH-reactive blood vessel (SSV) was detected on the SDH stain (arrowhead). (d) In patient 2, hematoxylin–eosin (a) and modified Gomori trichrome (b) stain revealed moderate fiber size variation without RRFs, SDH, (c) and COX statin (d) showed subsarcolemmal accumulation of mitochondria (arrows) without COX-negative fibers.

PCR-based sequencing method to avoid any adverse results associated with similar sequences in the nuclear DNA. The sequence data were compared with the Human DNA Revised Cambridge Reference Sequence (MITOMAP: a Human Mitochondrial Genome Database; http://www.mitomap.org/mitomap/mitoseq.html).

We devised a real-time PCR amplification method based on a previously described approach (Komaki et al., 2003) to accurately quantify the frequency of the 3244G > A mutation. The target sequence (np 3211–3322) was amplified using a pair of primers and two fluorogenic TaqMan™ probes (PE Applied Biosystems; Foster City, CA, USA) designed for the wild-type and mutant sequences (Table 1). The copy number of mtDNA containing each mutant or wild-type sequence was determined based on a standard curve created by the reaction of a known amount of plasmid containing the mtDNA fragment (np 3171–3350) with each wild-type or mutant sequence.

To identify the 3242G > A transition, we amplified the 126-bp PCR fragment with the forward and mismatched primers and digested the fragment by SacI. If the fragment did not have the 3242G > A base change, then 108- and 18-bp cleaved fragments would be obtained. Each fragment was detected in a 4% agarose gel (Nusieve 3:1 agarose; Bio-Whittaker Molecular Applications; Rockland, ME, USA) stained with ethidium bromide.

2.4. Biochemical studies of primary cultures and transmitochondrial cell lines

Primary skin fibroblasts were obtained from patients 1 and 2, and myoblasts could be obtained only from patient 2. The fibroblasts and myoblasts were grown in DMEM/F-12 medium with 20% fetal bovine serum (Invitrogen Corp. Carlsbad, CA, USA).

Transmitochondrial cell lines (cybrids) were obtained by polyethylene glycol fusing of enucleated fibroblasts from both patients with human osteosarcoma 143B/TK- cells lacking mtDNA (King and Attardi, 1989). Twenty clones derived from patient 2 were selected from a uridine-lacking medium and employed to measure ATP synthesis and enzymatic activity of individual mitochondrial respiratory complexes. The DNA was extracted from each clone for the quantification of the proportions of the 3244G > A mutation. Cybrid cells derived from patient 2 were used to measure enzymatic activity of individual mitochondrial respiratory complexes and for blue native polyacrylamide gel electrophoresis (BN-PAGE).

The methods to measure ATP synthesis in digitonin-permeabilized fibroblasts, myoblasts, or cybrids is described elsewhere (Komaki et al., 2003), along with several modifications of a method reported by Robinson (Robinson, 1996).

Enzymatic activity of individual mitochondrial respiratory complexes was performed on isolated mitochondria obtained from cultured 5×10^5 cybrid and 143B/TK-cells according to Trounce et al. with modifications (Trounce et al., 1996). The activities of complexes I, IV, and citrate synthase were measured by spectrophotometric assays as described. All samples were measured at least in duplicate and averaged.

Table 1
Fluoroeenie probes mid amplification primers for real-time PCR.

Fluorogenic probes sequence		Primer sequence
Wild	5′ (FAM)-TGGCAGA GCCCGGT-(MGB) p3′	Forward 5′-CCACCCAAGAACAGGGTTTG-3′
Mutant	5′ (VIC)-TGGCAGAACCCGGT-(MGB) p3′	Reverse 5′-GGTTGGCCATGGGTATGTTG-3′

The underlined positions corresponded to np 3244. MGB: minor groove binder.

2.5. BN-PAGE and Western blot for immunodetection

Mitochondrial proteins were isolated from cultured 143B/TK-cells and cybrids derived from patient 2 ($3–6 \times 10^6$ cells) (Nijtmans et al., 2002). The mitochondrial proteins (100 μg) were solubilized in sample buffer (Invitrogen) containing 0.5% (w/v) *n*-dodecyl-β-d-maltoside (DDM). Electrophoresis was performed on 3–12% polyacrylamide gels (Invitrogen) (Nijtmans et al., 2002; D'Aurelio et al., 2006). Following BN-PAGE, the gels were soaked in a transfer buffer (Invitrogen) and blotted onto polyvinylidene fluoride (PVDF) membranes using the iBlot transfer system (Invitrogen) according to the manufacturer's instructions (20 V, 7 min). Subunit-specific mouse monoclonal antibodies (Molecular Probes) were used to immunodetect protein complexes. The cocktail of primary antibodies included the 39 kDa (complex I, 0.5 μg/mL), 70 kDa (complex II, 0.5 μg/mL), core II (complex III, 0.5 μg/mL), subunit I (complex IV, 2.5 μg/mL), and subunit β (complex V, 0.5 μg/mL). After removing the cocktail of primary antibodies, the alkaline phosphatase-conjugated anti-mouse secondary antibody was reacted, and nitroblue tetrazolium chloride (NBT)-derived chromogenic detection was performed. We determined the appropriate conditions to solubilize the mitochondrial membranes while preserving the intact respiratory chain complexes.

3. Results

3.1. Histopathological study

The histopathological study of the skeletal muscle from patient 1, at the age of 6 years, revealed the presence of numerous ragged-red fibers (RRFs), i.e., ⩾15% of the total fibers and some strongly succinate dehydrogenase-reactive blood vessels (SSVs). The COX stain revealed diffuse COX-negative fibers, whereas most of the RRFs were reactive (Fig. 1B). In patient 2, at the age of 9 months, there was increased subsarcolemmal accumulation of mitochondria in many fibers, which suggested mitochondrial abnormalities, but typical RRF, SSV, and COX-negative fibers were not detected (Fig. 1C).

3.2. Molecular genetic studies

No large-scale mtDNA rearrangements were detected by the long PCR method in either patient. Total mtDNA sequencing of the muscle from patient 1 revealed 38 base changes compared with the revised standard sequence (Table 2). According to the MITOMAP database, 37 changes have been previously reported as normal polymorphisms. One of the observed changes was a G-to-A mutation at np 3244 in the mitochondrial $tRNA^{Leu(UUR)}$ gene, and this change appeared to be heteroplasmic (i.e., both the mutant and the wild-type genome were present) on electropherograms (Fig. 2A). Real-time PCR amplification confirmed that the percentage of mutant mtDNA in the patient's muscle and fibroblasts was 94% and 90%, respectively. In patient 2, total mtDNA sequencing of muscle revealed 41 base changes compared with the standard sequence (Table 3). According to the MITOMAP database, 39 changes have been previously reported as normal polymorphisms. We identified a 6481T > C base change that had not been reported previously to the MITOMAP database; however, we detected this base change in her healthy mother. We also detected a G-to-A base change at np 3242 (Fig. 2B). This change was confirmed by restriction fragment polymorphism and was revealed to be homoplasmic (i.e., only the mutant genome was present) in the patient's tissues, including blood, but was absent in the blood of her healthy mother (Fig. 2C). Total mtDNA sequencing of blood from the proband's mother revealed the

Table 2
MtDNA sequence variants in patient 1.

Gene product	np	Base-change	Amino acid change	MitoMap database
D-loop	73	A to G		Reported polymorphism
D-loop	152	T to C		Reported polymorphism
D-loop	263	A to G		Reported polymorphism
D-loop	311	Insertion C		Reported polymorphism
D-loop	489	T to C		Reported polymorphism
12S rRNA	750	A to G		Reported polymorphism
16S rRNA	2706	A to G		Reported polymorphism
16S rRNA	3010	G to A		Reported polymorphism
16S rRNA	3206	C to T		Reported polymorphism
tRNA-Leu(UUR)	3244	G to A		Unreported
NADH dehydrogenase 2	4763	A to G	Synonymous	Reported polymorphism
NADH dehydrogenase 2	4883	C to T	Synonymous	Reported polymorphism
NADH dehydrogenase 2	5178	C to A	L to M	Reported polymorphism
Cytochrome c oxydase I	7028	C to T	Synonymous	Reported polymorphism
ATP synthase a	8414	C to T	L to F	Reported polymorphism
ATP synthase a	8473	T to C	Synonymous	Reported polymorphism
ATP synthase 0	8701	A to G	T to A	Reported polymorphism
ATP synthase 0	8860	A to G	T to A	Reported polymorphism
Cytochrome c oxydase 3	9540	T to C	Synonymous	Reported polymorphism
Cytochrome c oxydase 3	9524	T to C	Synonymous	Reported polymorphism
NADH dehydrogenase 3	10308	A to G	T to A	Reported polymorphism
NADH dehydrogenase 3	10400	C to T	Synonymous	Reported polymorphism
tRNA-Arg	10410	T to C		Reported polymorphism
NADH dehydrogenase 4	10873	T to C	Synonymous	Reported polymorphism
NADH dehydrogenase 4	11710	G to A	Synonymous	Reported polymorphism
NADH dehydrogenase 5	12706	C to T	Synonymous	Reported polymorphism
NADH dehydrogenase 6	14068	C to T	Synonymous	Reported polymorphism
Cytochrome b	14766	C to T	I to T	Reported polymorphism
Cytochrome b	14783	T to C	Synonymous	Reported polymorphism
Cytochrome b	14070	T to C	I to T	Reported polymorphism
Cytochrome b	15043	G to A	Synonymous	Reported polymorphism
Cytochrome b	15301	G to A	Synonymous	Reported polymorphism
Cytochrome b	15314	G to A	A to T	Reported polymorphism
Cytochrome b	15326	A to G	T to A	Reported polymorphism
D-loop	16085	C to T		Reported polymorphism
D-loop	16120	G to A		Reported polymorphism
D-loop	10223	C to T		Reported polymorphism
D-loop	10223	T to C		Reported polymorphism
D-loop	10500	T to C		Reported polymorphism

same polymorphisms except for the 3242G > A base change (data not shown).

3.3. Biochemical studies

In patient 1, fibroblast ATP synthesis was significantly low when pyruvate/malate or glutamate/malate were used as the substrate (Fig. 2D), but the rate of synthesis was normal when succinate or TMPD/ascorbate were added to the cells. These findings revealed that fibroblasts derived from this patient had a complex I deficiency. To confirm that the 3244 mutation was pathogenic, we performed functional analysis of cybrids. We obtained 20 clones with a different percentage of the heteroplasmic np 3244 mutation and performed ATP synthesis assays using each clone. ATP synthesis was within the normal range when the percentage of mutant DNA remained under 90%. Clones carrying mutant mtDNA in high proportions, i.e., those exceeding the threshold level of approximately 95%, lost their ability to synthesize ATP when glutamate/malate or TMPD/ascorbate were used as the substrate (Fig. 2E,F). Moreover, analysis of enzymatic activity for individual mitochondrial respiratory complexes revealed that the activities of complexes I and II were apparently low in the cybrid cells carrying a high proportion of mutant mtDNA, although they were normal in cybrid cells carrying a low proportion of mutant mtDNA (Fig. 2G). These findings indicated that extremely high levels of the mutation led not only to a complex I deficiency, but also to complex IV and/or V deficiencies.

In contrast, the fibroblasts and myoblasts of patient 2 showed normal ATP synthesis (data not shown); however, her cybrid cells had low levels of complex IV activity (Fig. 2G).

3.4. Studies on assembly of respiratory chain enzymes

To understand the consequences of the 3242G > A mutation on the composition of the respiratory chain, BN-PAGE analysis was performed using the subunit-specific monoclonal antibodies on equal amounts of mitochondrial proteins extracted from the same number of mutant cybrids and human osteosarcoma 143B/TK- cells. Also, the amount of assembled respiratory chain complexes in cybrid clones carrying the 3242G > A mutation was estimated. Compared with 143B/TK-, cybrids showed a reduced level of the complex I-III-IV supercomplex and an increase in the amount of the complex I-III supercomplex. The levels of the complex III homodimer and complex II were assessed as a loading control (Fig. 2H).

4. Discussion

MELAS is a maternally inherited disorder typically characterized by onset before the age 15 years, lactic acidosis, episodic vomiting, seizures, migraine-like headaches, and recurrent cerebral insults resembling strokes (Goto, 1995; Hirano and Pravlakis, 1994). The symptoms of patient 1, including the onset age, recurrent episodic vomiting, headache, hemiconvulsions, and severe lactic acidosis, were consistent with the clinical spectrum associated

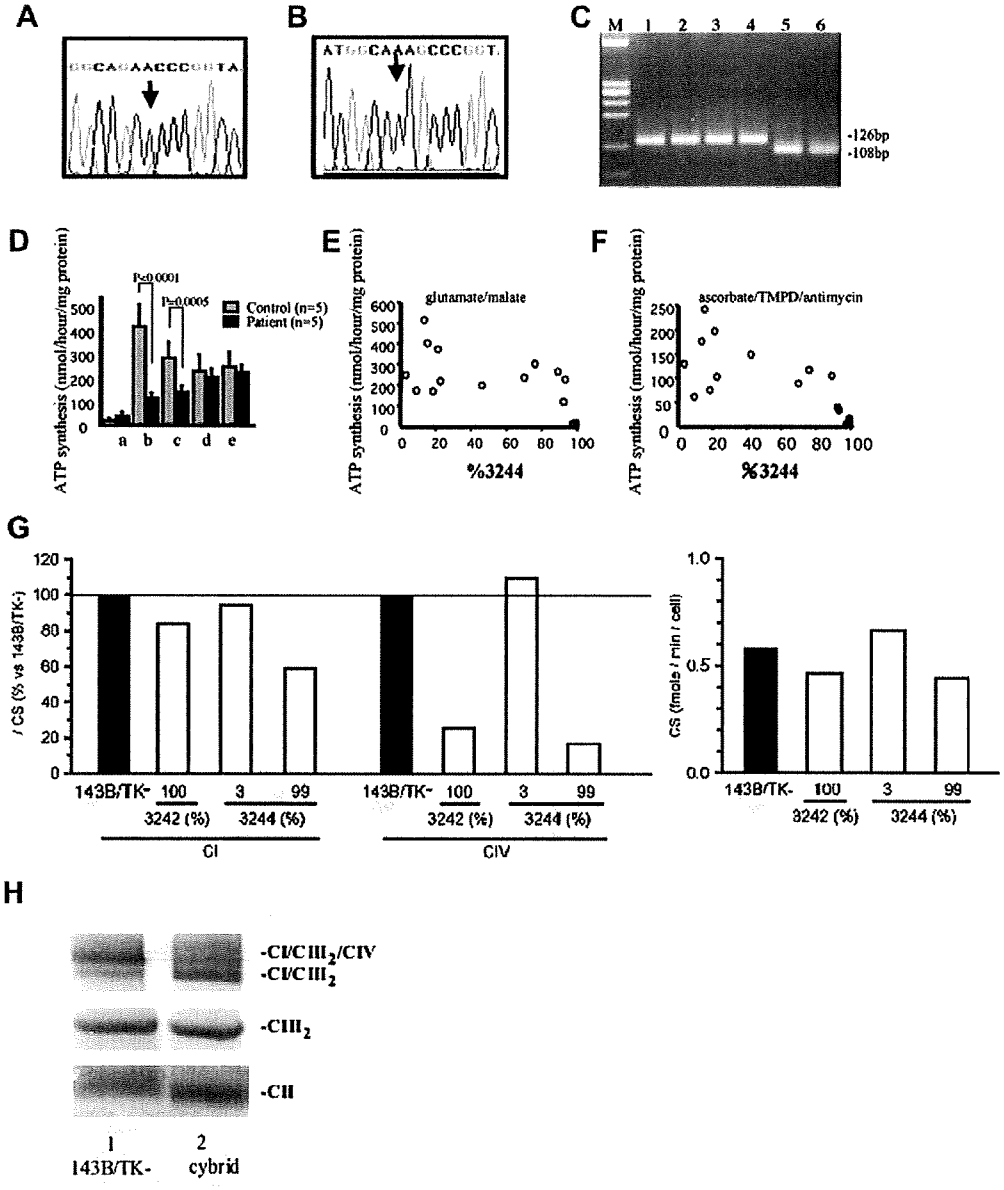

Fig. 2. Molecular and biochemical analysis. (A) An electropherogram based on mtDNA sequencing from muscle specimens revealed a heteroplasmic G-to-A substitution at nucleotide position 3244 (arrow) in the $tRNA^{Leu(UUR)}$ gene of patient 1, and a (B) G-to-A substitution at nucleotide position 3242 (arrow) in patient 2. (C) SacI digestion of the mutant 3242G > A mtDNA is indicated by a 126-bp band. Wild-type mtDNA is indicated by the presence of a 108-bp band. M, molecular weight markers; lane 1, patient's muscle; lane 2, myoblast; lane 3, fibroblast; lane 4, blood; lane 5, mother's blood; lane 6, wild-type control. (D) ATP synthesis in a digitonin-treated primary culture of fibroblasts with 90% mutants. ATP synthesis was measured using the following combinations of substrates and specific inhibitors: a, none; b, pyruvate/malate; c, glutamate/malate; d, succinate/rotenone; e, ascorbate/TMPD/antimycin. The results of this assay are expressed as nanomoles ATP per hour per milligram of cell protein. The control values are presented as the mean ±1 SD. ATP synthesis in 143B/TK- derived cybrid clones with various percentages of the 3244G > A mutation (open circles) and 143B/TK- cells (closed circles). (E) Glutamate + malate was used as the substrate. (F) Ascorbate and TMPD were used as the substrates, and antimycin was used as an inhibitor. (G) Activities of the respiratory chain complexes relative to citrate synthase in 143B/TK- cells and cybrid clones carrying the 3242G > A mutation (100% mutant) and the 3244G > A mutation (3% and 99% mutant). The figure to the right shows the activity of citrate synthase in these clones. CI, complex I; CIV, complex IV; CS, citrate synthase. (H) $CI/CIII_2/CIV$ supercomplex level decreases and $CI/CIII_2$ supercomplex level increases in cybrid clones carrying the 3242G > A mutation (lane 2), compared to 143B/TK-cells (lane 1). $CI/CIII_2/CIV$, complex I-III-IV supercomplex; $CI/CIII_2$, complex I-III supercomplex; $CIII_2$, complex III homodimer; CII, monomeric complex II.

with MELAS. Morphological analysis of the muscle biopsy also showed typical findings of MELAS. We detected diffuse COX-negative fibers and numerous RRFs, some of which stained positive for COX activity, as has previously been reported in MELAS patients but not in those with other mitochondrial myopathies (Goto et al., 1992). We also observed SSVs, which is an important finding in MELAS patients (Hasegawa et al., 1991). Patient 2 showed multiple tissue involvement including severe lactic acidosis, cardiomyopathy, renal tubular dysfunction, cerebral atrophy, generalized hypotonia in infancy, and increased subsarcolemmal accumulation of mitochondria in the muscle biopsy, which strongly suggested that she had a mitochondrial disease. However, the clinical picture and pathological findings were apparently different from MELAS.

The underlying molecular defects involved in these cases were distinct from the common causes of mitochondrial disorders including MELAS. Here, none of the previously reported pathogenic

Table 3
MtDNA sequence variants m patient 2.

Gene product	np	Base change	Amino acid change	MitoMap database
D-loop	73	A to G		Reported polymorphism
D-loop	152	T to C		Reported polymorphism
D-loop	263	A to G		Reported polymorphism
D-loop	303	Insertion C		Reported polymorphism
D-loop	311	Insertion C		Reported polymorphism
D-loop	480	T to C		Reported polymorphism
12S rRNA	750	A to G		Reported polymorphism
12S rRNA	1438	A to G		Reported polymorphism
16S rRNA	2706	A to G		Reported polymorphism
16S rRNA	3010	G to A		Reported polymorphism
16S rRNA	3206	C to T		Reported polymorphism
tRNA-Leu(UUR)	3242	G to A		Unreported
NADH dehydrogenase 2	4760	A to G	Synonymous	Reported polymorphism
NADH dehydrogenase 2	4883	C to T	Synonymous	Reported polymorphism
NADH dehydrogenase 2	5173	C to A	L to M	Reported polymorphism
NADH dehydrogenase 2	5201	G to A	A to T	Reported polymorphism
Cytochrome c oxydase I	6481	T to C	V to A	Unreported
Cytochrome c oxydase I	7028	C to T	Synonymous	Reported polymorphism
ATP synthase 8	8414	C to T	L to F	Reported polymorphism
ATP synthase 8	8473	T to C	Synonymous	Reported polymorphism
ATP synthase 6	3701	A to G	T to A	Reported polymorphism
ATP synthase 6	8860	A to G	T to A	Reported polymorphism
Cytochrome c oxydase 3	8540	T to C	Synonymous	Reported polymorphism
NADH dehydrogenase 3	10,308	A to G	T to A	Reported polymorphism
NADH dehydrogenase 3	10,400	C to T	Synonymous	Reported polymorphism
tRNA-Arg	10,410	T to C		Reported polymorphism
NADH dehydrogenase 4	10,873	T to C	Synonymous	Reported polymorphism
NADH dehydrogenase 4	11,710	G to A	Synonymous	Reported polymorphism
NADH dehydrogenase 5	12,706	C to T	Synonymous	Reported polymorphism
NADH dehydrogenase 6	14,068	C to T	Synonymous	Reported polymorphism
Cytochrome b	14,766	C to T	I to T	Reported polymorphism
Cytochrome b	14,783	T to C	Synonymous	Reported polymorphism
Cytochrome b	14,870	T to C	I to T	Reported polymorphism
Cytochrome b	15,043	G to A	Synonymous	Reported polymorphism
Cytochrome b	15,301	G to A	Synonymous	Reported polymorphism
Cytochrome b	15,314	G to A	A to T	Reported polymorphism
Cytochrome b	15,320	A to G	T to A	Reported polymorphism
D-loop	16,120	G to A		Reported polymorphism
D-loop	16,223	C to T		Reported polymorphism

The T64S1C base change was observed in a healthy mother of patient 2.

mutations of mtDNA were found, but we did identify base changes adjacent to the 3243A > G mutation, which is the most common mutation in MELAS patients, including a 3244G > A transition in patient 1 and a 3242G > A transition in patient 2 (Fig. 3A). The 3244G > A and 3242G > A base changes have not been reported clinically, but as a somatic mutation in gastric carcinoma (Habano et al., 2000) and in the bone marrow of a patient with myelodysplastic syndrome (Gattermann et al., 2004), respectively.

Several lines of evidence support a causal association between the 3244G > A base change mutation and MELAS. First, this base change was not observed in over 200 normal individuals. Second, the 3244G > A transition disrupted a highly conserved nucleotide in the tRNA structure (Fig. 3B). Third, most mutations in typical cases of MELAS were located in the same tRNA gene, including the 3271T > C (Goto et al., 1991), 3291T > C (Goto et al., 1994), 3252A > G (Morten et al., 1993), and 3260A > G mutations (Nishino et al., 1996). Moreover, the 3244G > A base change was located adjacent to the most common mutation in MELAS patients, namely, the 3243A > G mutation (Fig. 3A). Fourth, this mutation existed under heteroplasmic conditions, which is a common feature of pathogenic mtDNA mutations. Finally, a functional analysis of cybrids revealed a significant decrease in the respiratory chain function, which was observed in cells with a relatively high percentage of mutant mtDNA. The results of these assays indicated deficiencies of complexes I and IV and a threshold effect of mutant load on respiratory chain enzyme activity, which has often been observed in MELAS patients carrying the 3243A > G mutation (Goto, 1995; Koga et al., 1995).

In patient 2, 6481T > C and 3242G > A base changes were detected; these polymorphisms were not reported previously. The 6481T > C change resulted in the replacement of valine with alanine; however, we detected this base change in her healthy mother. Therefore, it is reasonable to conclude that this base change is not pathogenic. In patient 2, the 3242G > A base change existed in all tissues in a homoplasmic condition, which is different than the 3244G > A or the more common 3243A > G mutation (Fig. 2C), thus making its pathogenicity difficult to confirm. However, there is evidence, including the biochemical defects in cybrid cells, to support the pathogenicity of this base change (Chinnery et al., 1999; McFarland et al., 2004). First, this transition was segregated with the disease; it was not detected in more than 200 normal individuals. Moreover, it was not detected in the blood of her healthy mother, although the base change was present in blood of the proband (Fig. 2C). Second, the 3242G > A transition affected a highly conserved position in the $tRNA^{Leu(UUR)}$ gene (Fig. 3B). Third, pathogenic mutations of several mitochondrial diseases have involved the dihydrouridine (DHU) stem of this tRNA (Kawarai et al., 1997; Nishigaki et al., 2003; Hao and Moraes, 1996). It is important to note that the DHU stem appears to be a rather weak structure and might thus be more prone to alterations leading to structural disturbances. The 3242G > A transition can alter the secondary and possibly the tertiary structure of the DHU-stem due to

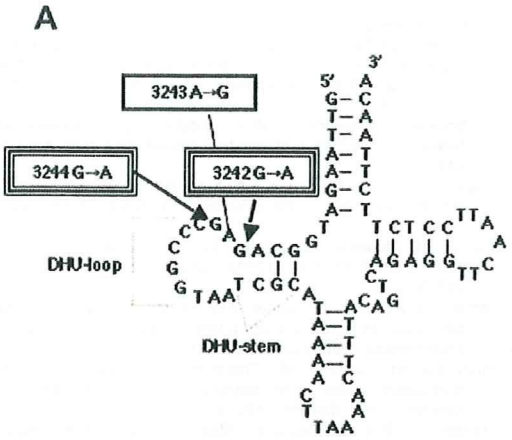

B

	Acc-stem		D-stem	D-loop	D-stem
Patient 1	GTTAAGA	TG	GCAG	A[A]CCCGGTAA	TCGC
Patient 2	GTTAAGA	TG	GCA[A]	AGCCCGGTAA	TCGC
Homo sapiens	GTTAAGA	TG	GCAG	AGCCCGGTAA	TCGC
Balaenoptera musculus	GTTAAGA	TG	GCAG	AGCCCGGTAA	TCGC
Bos taurus	GTTAAGG	TG	GCAG	AGCCCGGTAA	TTGC
Didelphis virginiana	ATTAAGG	TG	GCAG	AGAAGGTAA	TCGC
Equus caballus	GTTAAGG	TG	GCAG	AGCCCGGAAA	TTGC
Gorilla gorilla	GTTAAGA	TG	GCAG	AGCCCGGTAA	TCGC
Hylobates lar	GTTAAGA	TG	GCAG	AGCCCGGCAA	TTGC
Mus musculus	ATTAGGG	TG	GCAG	AGCCAGGAAA	TTGC
Oryctolagus cuniculus	GTTAAGG	TG	GCAG	AGCCCGTAA	TTGC
Pan troglodytes	GTTAAGA	TG	GCAG	AGCCCGGTAA	TTGC
Pongo pygmaeus	GTTAAGA	TG	GCAG	AGCCCGGTAA	TTGC
Rattus norvegicus	ATTAGGG	TG	GCAG	AGCCAAGTAA	TTGC
Xeno laevis	GCTAGCG	TG	GCAG	AGCCTGGTAA	TGCG

Fig. 3. (A) Secondary structure of the human mitochondrial tRNA$^{Leu(UUR)}$ gene and positions of the 3242G > A, 3243A > G, and 3244G > A mutations. (B) Comparison of mitochondrial tRNA$^{Leu(UUR)}$ among several species. 3242G > A and 3244G > A mutations are boxed.

"strengthening" of the stem by the formation of an additional A–U pairing instead of the well-conserved C–U pair (Helm et al., 2000) (Fig. 3A). Fourth, a somatic mutation of the 3242G > A was recently detected in CD34+ bone marrow cells, but not in peripheral blood cells (Gattermann et al., 2004). The authors supported the pathogenicity of this mutation, which they thought was associated with a maturation defect, and that the dysfunction of the mitochondria carrying the mutation contributed to ineffective hematopoiesis in their patient. Finally, we found that the cybrid cells carrying the 3242G > A mutation derived from patient 2, which excluded any influence of nuclear genes, revealed the functional defect of the mutation; the enzymatic activity of complex IV was apparently low in cybrid cells and the BN-PAGE analysis of the cybrid cells showed a reduced level of the complex I–III–IV supercomplex and an increase in the complex I–III supercomplex. Recently, an abnormal respiratory supercomplex was reported in a human disease (McKenzie et al., 2006). They proposed that unstable respiratory chain supercomplexes affect respiratory activities and subsequent pathology. In our case, the above findings suggest that the destabilization of the supercomplex due to the dissociation of complex IV is related to the activity of complex IV.

Point mutations at many of the 75 nucleotides in the tRNA $^{Leu(UUR)}$ gene have been associated with several distinct mitochondrial diseases with variable phenotypes ranging from pure myopathy to multisystemic disorders such as MELAS (Campos et al., 2001; Hadjigeorgiou et al., 1999; Goto et al., 1990; Sevidei, 2002; Moraes et al., 1992; Seneca et al., 2001; Jaksch et al., 2001). However, the reasons for the differences between the genotypes and phenotypes are not clear. The novel 3244G > A mutation emphasizes the crucial role of tRNA$^{Leu(UUR)}$ dysfunction in the pathogenesis of MELAS. Because its biochemical effects were similar to those of the 3243A > G mutation, this portion of the tRNA gene is likely to be very important for the maintenance of tRNA function. However, the effects of the 3242G > A base change in the DHU stem on the clinical phenotype, pathological findings, and biochemical functions are different from those of the 3243A > G mutation. Because both novel base changes are adjacent to the common 3243A > G mutation, these different effects may be a key to clarify the molecular pathogenesis of mitochondrial disorders including MELAS.

Regarding the pathogenesis of the tRNA$^{Leu(UUR)}$ gene mutations including the 3243A > G mutation, several groups have pointed out the possibility of an abnormality at the transcription level, because these mutations occur in a control region responsible for the termination of transcription at the end of rRNA genes (Hess et al., 1991; King et al., 1992). Other groups have demonstrated that this type of mutant tRNA may be functionally deficient (Yasukawa et al., 2000; Chomyn et al., 2000). One of the groups revealed a specific correlation between the modification deficiency in mutant tRNA and the clinical features of mitochondrial disorders (Kirino et al., 2005). They reported that mitochondrial tRNA$^{Leu(UUR)}$ harboring mutations, such as the 3244G > A transition, detected in tissues from patients with symptoms of MELAS lacked the normal taurine-containing modification at the anticodon wobble position. In contrast, mitochondrial tRNA $^{Leu(UUR)}$ with mutations, including the 3242G > A transition, detected in patients that have mitochondrial diseases but do not show the MELAS symptoms had the normal modifications. Further investigations of the different effects of the np 3244 and np 3242 base changes on the phenotypes and the similarities shared by the np 3243 and 3244 base changes may provide clues for elucidating the actual impact of tRNA $^{Leu(UUR)}$ gene mutations on the phenotypic expression of MELAS. The present results can contribute to a better understanding of tRNA function and provide insight into the complicated issues surrounding the association between genotype and phenotype in mitochondrial disorders.

Acknowledgements

We thank Mayuko Kato, Mitsuko Tanabe, and Munemitsu Yuasa for technical assistance. This work was supported in part by a Research Grant (15B-4, 18A-5) for Nervous and Mental Disorders from the Ministry of Health, Labor and Welfare of Japan (Y.G.), and a grant of the Comprehensive Research Project on Health Sciences Focusing on Drug Innovation (KHD2207) from the Japan Health Sciences Foundation (Y.G.).

References

Akanuma, J., Muraki, K., Komaki, H., Nonaka, I., Goto, Y., 2000. Two pathogenic point mutations exist in the authentic mitochondrial genome, not in the nuclear pseudogene. J. Hum. Genet. 45, 337–341.

Campos, Y., Gamez, J., Garcia, A., Andreu, A.L., Rubio, J.C., Martin, M.A., del Hoyo, P., Navarro, C., Cervera, C., Garesse, R., Arenas, J., 2001. A new mtDNA mutation in the tRNA$^{Leu(UUR)}$ gene associated with ocular myopathy. Neuromuscul. Disord. 1, 477–480.

Chinnery, P.F., Howell, N., Andrews, R.M., Turnbull, D.M., 1999. Mitochondria DNA analysis: polymorphisms and pathogenicity. J. Med. Genet. 36, 505–510.

Chomyn, A., Martinuzzi, A., Yoneda, M., Daga, A., Hurko, O., Johns, D., Lai, S.T., Nonaka, I., Angelini, C., Attardi, G., 1992. MELAS mutation in mtDNA binding site for transcription termination factor causes defects in protein synthesis and in respiration but no change in levels of upstream and downstream mature transcripts. Proc. Natl. Acad. Sci. USA 89, 4221–4225.

Chomyn, A., Enriquez, J.A., Micol, V., Fernandez-Silva, P., Attardi, G., 2000. The mitochondrial myopathy, encephalopathy, lactic acidosis, and stroke-like

episode syndrome-associated human mitochondrial tRNA$^{Leu(UUR)}$ mutation causes aminoacylation deficiency and concomitant reduced association of mRNA with ribosomes. J. Biol. Chem. 275, 19198–19209.

D'Aurelio, M., Gajewski, C.D., Lenaz, G., Manfredi, G., 2006. Respiratory chain supercomplexes set the threshold for respiration defects in human mtDNA mutant cybrids. Hum. Mol. Genet. 15, 2157–2169.

Gattermann, N., Wulfert, M., Junge, B., Germing, U., Haas, R., Hofhaus, G., 2004. Ineffective hematopoiesis linked with a mitochondrial tRNA mutation (3242G > A) in a patient with myelodysplastic syndrome. Blood 103, 1499–1502.

Goto, Y., 1995. Clinical features of MELAS and mitochondrial DNA mutations. Muscle Nerve 3, S107–112.

Goto, Y., Nonaka, I., Horai, S., 1990. A mutation in the tRNA$^{Leu(UUR)}$ gene associated with the MELAS subgroup of mitochondrial encephalopathies. Nature 348, 651–653.

Goto, Y., Nonaka, I., Horai, S., 1991. A new mtDNA mutation associated with mitochondrial myopathy, encephalopathy, lactic acidosis, and stroke-like episodes (MELAS). Biochim. Biophys. Acta 1097, 238–240.

Goto, Y., Horai, S., Matsuoka, T., Koga, Y., Nihei, K., Kobayashi, M., Nonaka, I., 1992. Mitochondrial myopathy, encephalopathy, lactic acidosis, and stroke-like episodes (MELAS): a correlative study of the clinical features and mitochondrial DNA mutation. Neurology 42, 545–550.

Goto, Y., Tsugane, K., Tanabe, Y., Nonaka, I., Horai, S., 1994. A new point mutation at nucleotide pair 3291 of the mitochondrial tRNA$^{Leu(UUR)}$ gene in a patient with mitochondrial myopathy, encephalopathy, lactic acidosis, and stroke-like episodes (MELAS). Biochem. Biophys. Res. Commun. 202, 1624–1630.

Habano, W., Sugai, T., Nakamura, S.I., Uesugi, N., Yoshida, T., Sasou, S., 2000. Microsatellite instability and mutation of mitochondrial and nuclear DNA in gastric carcinoma. Gastroenterology 118, 835–841.

Hadjigeorgiou, G.M., Kim, S.H., Fischbeck, K.H., Andreu, A.L., Berry, G.T., Bingham, P., Shanske, S., Bonilla, E., DiMauro, S., 1999. A new mitochondrial DNA mutation (A3288G) in the tRNA$^{Leu(UUR)}$ gene associated with familial myopathy. J. Neurol. Sci. 164, 153–157.

Hao, H., Moraes, C.T., 1996. Functional and molecular mitochondrial abnormalities associated with C->T transition at position 3256 of the human mitochondrial genome. J. Biol. Chem. 271, 2347–2352.

Hasegawa, H., Matsuoka, T., Goto, Y., Nonaka, I., 1991. Strongly succinate dehydrogenase-reactive blood vessels in muscles from patients with mitochondrial myopathy, encephalopathy lactic acidosis, and stroke-like episodes. Ann. Neurol. 29, 601–605.

Helm, M., Brule, H., Friede, D., Giege, R., Putz, D., Florentz, C., 2000. Search for characteristic structural features or mammalian mitochondrial tRNAs. RNA 6, 1356–1379.

Hess, J.F., Parisi, M.A., Bennett, J.L., Clayton, D.A., 1991. Impairment of mitochondrial transcription termination by a point mutation associated with the MELAS subgroup of mitochondrial encephalomyopathies. Nature 351, 236–239.

Hirano, M., Pravlakis, S., 1994. Mitochondrial myopathy, encephalopathy, lactic acidosis, and stroke-like episodes (MELAS): current concepts. J. Child Neurol. 9, 4–13.

Jaksch, M., Lochmuller, H., Schmitt, F., Volpel, B., Obermaier-Kusser, B., Horvath, R., 2001. A mutation in mt tRNA$^{Leu(UUR)}$ causing a neuropsychiatric syndrome with depression and cataract. Neurology 57, 1930–1931.

Kawarai, T., Kawakami, H., Kozuka, K., Izumi, Y., Matsuyama, Z., Watanabe, C., Kohriyama, T., Nakamura, S., 1997. A new mitochondrial DNA mutation associated with mitochondrial myopathy: tRNA$^{Leu(UUR)}$ 3254C-to-G. Neurology 49, 598–600.

King, M.P., Attardi, G., 1989. Human cells lacking mtDNA: repopulation with exogenous mitochondria by complementation. Science 246, 500–503.

King, M.P., Koga, Y., Davidson, M., Schon, E.A., 1992. Defects in mitochondrial protein synthesis and respiratory chain activity segregate with the tRNA$^{Leu(UUR)}$ mutation associated with mitochondrial myopathy, encephalopathy, lactic acidosis, and stroke-like episodes. Mol. Cell Biol. 12, 480–490.

Kirino, Y., Goto, Y., Campos, Y., Arenas, J., Suzuki, T., 2005. Specific correlation between the wobble modification deficiency in mutant tRNAs and the clinical features of a human mitochondrial disease. Proc. Natl. Acad. Sci. USA 102, 7127–7132.

Koga, Y., Davidson, M., Schon, E.A., King, M.P., 1995. Analysis of cybrids harboring MELAS mutations in the mitochondrial tRNAs$^{Leu(UUR)}$ gene. Muscle Nerve 3, S119–123.

Komaki, H., Akauma, J., Iwata, H., Takahashi, T., Mashima, Y., Nonaka, I., Goto, Y., 2003. A novel mtDNA C11777A mutation in Leigh syndrome. Mitochondrion 2, 293–304.

McFarland, R., Elson, J.L., Taylor, R.W., Howell, N., Turnbull, D.M., 2004. Assigning pathogenicity to mitochondrial tRNA mutations: when 'definitely maybe' is not good enough. Trends Genet. 20, 591–596.

McKenzie, M., Lazarou, M., Thorborn, D.R., Ryan, M.T., 2006. Mitochondrial respiratory chain supercomplexes are destabilized in Barth syndrome patients. J. Mol. Biol. 361, 462–469.

Moraes, C.T., Ricci, E., Bonilla, E., DiMauro, S., Schon, E.A., 1992. The mitochondrial tRNA$^{Leu(UUR)}$ mutation in mitochondrial encephalomyopathy, lactic acidosis, and stroke-like episodes (MELAS): genetic, biochemical, and morphological correlation in skeletal muscle. Am. J. Hum. Genet. 50, 934–949.

Morten, K.J., Cooper, J.M., Brown, G.K., Lake, B.D., Pike, D., Poulton, J., 1993. A new point mutation associated with mitochondrial encephalomyopathy. Hum. Mol. Genet. 2, 2081–2087.

Nijtmans, L.G., Henderson, N.S., Holt, I.J., 2002. Blue native electrophoresis to study mitochondrial and other protein complexes. Methods 26, 327–334.

Nishigaki, Y., Tadesse, S., Bonilla, E., Shungu, D., Hersh, S., Keats, B.J., Berlin, C.I., Goldverg, M.F., Vockley, J., DiMauro, S., Hirano, M., 2003. A novel mitochondrial tRNA$^{Leu(UUR)}$ mutation in a patient with features of MERRF and Kearns-Sayre syndrome. Neuromuscul. Disord. 13, 334–340.

Nishino, I., Komatsu, M., Kodama, S., Horai, S., Nonaka, I., Goto, Y., 1996. The 3260 mutation in mitochondrial DNA can cause mitochondrial myopathy, encephalopathy, lactic acidosis, and stroke-like episodes (MELAS). Muscle Nerve 19, 1603–1604.

Robinson, B.H., 1996. Use of fibroblast and lymphoblast cultures for detection of respiratory chain defects. In: Attardi, G.M., Chomyin, A. (Eds.), Methods in Enzymology, No. 264. Academic Press USA, San Diego, CA, pp. 454–463.

Sakuta, R., Nonaka, I., 1989. Vascular involvement in mitochondrial myopathy. Ann. Neurol. 25, 594–601.

Seneca, S., Verhelst, H., De Meirleir, L., Meire, F., Ceuterick-De Goote, C., Lissens, W., Van Coster, R., 2001. A new mitochondrial point mutation in the transfer RNA$^{Leu(UUR)}$ gene in a patient with a clinical phenotype resembling Kearn-Sayre syndrome. Arch. Neurol. 58, 1113–1118.

Sevidei, S., 2002. Mitochondrial encephalomyopathies: gene mutation. Neuromuscul. Disord. 12, 524–529.

Suzuki, T., Suzuki, T., Wada, T., Saigo, K., Watanabe, K., 2002. Taurine as a constituent of mitochondrial tRNAs: new insights into the functions of taurine and human mitochondrial diseases. EMBO J. 21, 6581–6589.

Trounce, I.A., Kim, Y.L., Jun, A.S., Wallace, D.C., 1996. Assessment of mitochondrial oxidative phosphorylation in patient muscle biopsies, lymphoblasts, and transmitochondrial cell lines. In: Attardi, G.M., Chomyin, A. (Eds.), Methods in Enzymology, No. 264. Academic Press USA, San Diego, CA, pp. 484–509.

Yasukawa, T., Suzuki, T., Ueda, T., Ohta, S., Watanabe, K., 2000. Modification defect at anticodon wobble nucleotide of mitochondrial tRNAs$^{Leu(UUR)}$ with pathogenic mutations of mitochondrial myopathy, encephalopathy, lactic acidosis, and stroke-like episodes. J. Biol. Chem. 275, 4251–4257.

[Autophagy 5:6, 795-804; 16 August 2009]; ©2009 Landes Bioscience

Research Paper

Autophagic degradation of nuclear components in mammalian cells

Young-Eun Park,[1,2] Yukiko K. Hayashi,[1,*] Gisèle Bonne,[3,4] Takuro Arimura,[5] Satoru Noguchi,[1] Ikuya Nonaka[1] and Ichizo Nishino[1]

[1]Department of Neuromuscular Research; National Institute of Neuroscience; National Center of Neurology and Psychiatry (NCNP); Kodaira, Tokyo Japan; [2]Department of Neurology and Medical Research Institute; Pusan National University Hospital; Seo-gu, Busan Korea; [3]Inserm-UPMC-CNRS UMRS_974; Institut de Myologie Paris; France; [4]AP-HP; Groupe Hospitalier Pitié-Salpêtrière; U.F. Cardiogénétique et Myogénétique; Service de Biochimie Métabolique; Paris, France; [5]Department of Molecular Pathogenesis; Medical Research Institute; Tokyo Medical and Dental University; Tokyo, Japan

Abbreviations: DAPI, 4',6-diamidino-2-phenylindole; GFP, green fluorescent protein; LC3, microtubule-associated protein 1 light chain 3; LC3-I, unlipidated form of LC3; LC3-II, lipidated form of LC3 (LC3-phopholipid conjugate); PI3K, phosphatidylinositol-3 kinase

Key words: autophagy, nuclear envelopathies, A-type lamins, emerin, nucleus

Autophagy is an evolutionarily conserved intracellular mechanism for the degradation of organelles and proteins. Here we demonstrate the presence of perinuclear autophagosomes/autolysosomes containing nuclear components in nuclear envelopathies caused by mutations in the genes encoding A-type lamins (*LMNA*) and emerin (*EMD*). These autophagosomes/autolysosomes were sometimes bigger than a nucleus. The autophagic nature is further supported by upregulation of LC3-II in *Lmna*$^{H222P/H222P}$ fibroblasts. In addition, inhibition of autophagy led to the accumulation of nuclear abnormalities and reduced cell viability, strongly suggesting a beneficial role of autophagy, at least in these cells. Similar giant autophagosomes/autolysosomes were seen even in wild-type cells, albeit rarely, implying that this "nucleophagy" is not confined to the diseased condition, but may be seen even in physiologic conditions to clean up nuclear wastes produced by nuclear damage.

Introduction

Nuclear envelopathies refer to disorders caused by mutations in the genes encoding nuclear envelope proteins, such as A-type lamins (*LMNA*) and emerin (*EMD*). *LMNA* mutations are known to cause a heterogeneous group of disorders collectively called as laminopathies, which encompass autosomal dominant and recessive forms of Emery-Dreifuss muscular dystrophy (AD and AR-EDMD), limb girdle muscular dystrophy type 1B (LGMD1B), cardiomyopathy with conduction defects, partial lipodystrophy, Charcot-Marie-Tooth disease type 2, and premature aging syndrome.[1-9] *EMD* mutations are causative for emerinopathies, a group of disorders that include X-linked EDMD, LGMD, cardiomyopathy with conduction defects, and familial atrial fibrillation.[10-13]

Because lamins form a protein meshwork of nuclear lamina at the nucleoplasmic side of inner nuclear membrane and have an important role in the maintenance of nuclear architecture, mutations in *LMNA* are thought to cause nuclear membrane fragility. This phenomenon is expected especially in skeletal and cardiac muscle cells which are constantly subjected to repeated mechanical stress. Loss of A-type lamins has been implicated to impair nuclear mechanics and increase nuclear fragility.[14,15] Loss of emerin, an inner nuclear membrane protein, could also lead to structural instability of nuclear membrane; emerin binds to several structural proteins in nucleus such as lamins, nesprins and nuclear actin, and can promote actin polymerization in vitro.[16-19]

In skeletal and cardiac muscles from patients with laminopathy and emerinopathy, various nuclear abnormalities have been observed, which are mainly composed of alteration in nuclear shape and emphasizing the role of lamins in the maintenance of nuclear integrity.[20-24] We recently demonstrated the presence of unique perinuclear vacuolar structures in the skeletal and/or cardiac muscles from laminopathy patients and emerin-null mice under electron microscopy,[21,25] but neither the nature of these structures nor their role in disease pathomechanism have ever been clarified. As most of these vacuolar structures contained amorphous and electron-dense materials resembling myelinated materials, we suspected that these are actually autophagic in nature.

Macroautophagy is a well-conserved molecular mechanism for the bulk degradation of organelles and proteins.[26-28] During autophagic process a double-membraned structure, the so-called phagophore or preautophagosome, randomly engulfs cytosolic components and cellular organelles. It is enclosed to form the so-called autophagosome, which is then fused with lysosome enabling intra-autophagosomal components to be degraded by lysosomal hydrolases.[28]

Recently it has been alluded to that the autophagic process is also responsible for selective degradation of specific cellular

*Correspondence to: Yukiko K. Hayashi; National Institute of Neuroscience, NCNP; 4-1-1 Ogawa-Higashi; Kodaira, Tokyo 187-8502 Japan; Tel.: 81.42.341.2711 Ex. 5113; Fax: 81.42.346.1742; Email: hayasi_y@ncnp.go.jp

Submitted: 11/17/08; Revised: 04/20/09; Accepted: 04/30/09

Previously published online as an *Autophagy* E-publication: http://www.landesbioscience.com/journals/autophagy/article/8901

components; for instance, pexophagy works to decrease the number of peroxisome adapting to environmental changes in yeast, while mitophagy and ER-phagy have been suggested to degrade damaged mitochondria and overstressed endoplasmic reticulum, respectively.[29-31]

In this study, we show that the perinuclear vacuolar structures are actually giant autophagosomes/autolysosomes involved in the degradation of damaged nuclear components, extending the concept of macroautophagy in various cellular organelles to include the nucleus.

Results

Perinuclear vacuolar structures observed in skeletal and cardiac muscles of human and mouse nuclear envelopathy. Electron microscopic observation of skeletal muscles from patients with laminopathy revealed perinuclear vacuolar structures in ~10% of myonuclei.[21] Most of these structures were consistently found in close proximity to the irregularly-shaped nuclei which also contained disorganized chromatin structures. These vacuolar structures varied in size from 1.5 to 5 μm in diameter, and were observed to contain either diffuse granular, honeycomb-like or dense amorphous materials within multiple layered and folded membranes (Fig. 1A and B). Similar structures were also observed near the nuclei of nonmuscle cells from muscle specimens (Fig. 1C).

Perinuclear vacuolar structures were also detected in skeletal and cardiac muscles from different mouse models of nuclear envelopathies including emerin lacking *Emd*$^{-/-}$ (89 weeks of age),[25] A-type lamin-deficient *Lmna*$^{-/-}$ (10 weeks), and homozygous knock-in *Lmna*$^{H222P/H222P}$ (24 weeks) mouse models (Fig. S1), and also in skin fibroblasts from 10-week-old *Lmna*$^{H222P/H222P}$ mouse (Fig. 1D).

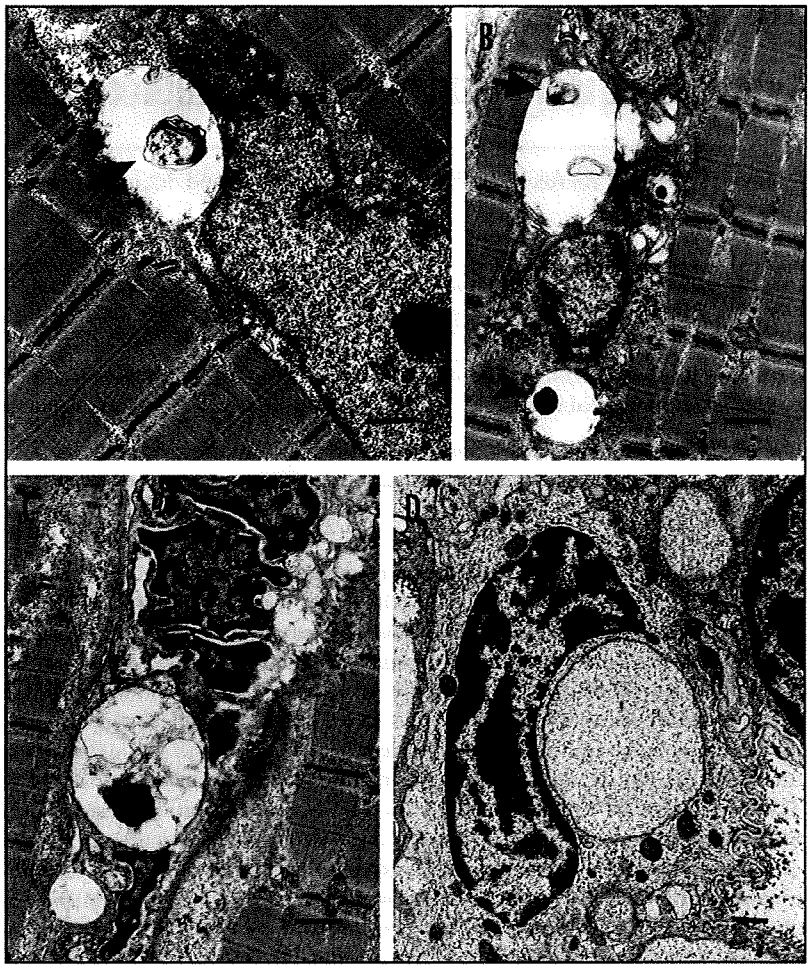

Figure 1. Electron microscopic observation of perinuclear vacuolar structures in skeletal muscles from patients (A–C) and skin from *Lmna*$^{H222P/H222P}$ mouse (D). (A–C) Perinuclear vacuolar structures of variable diameter usually contain myelinated (arrows) and dense amorphous materials (arrowhead) in muscle (A and B) and nonmuscle cells in skeletal muscle specimens (C) of patients with AD-EDMD/LGMD1B. (D) In the skin obtained from 10-week-old *Lmna*$^{H222P/H222P}$ mouse, similar perinuclear vacuolar structures are observed. Bars, 0.5 μm.

Electron microscopic observation of *Lmna*$^{H222P/H222P}$ MEF. For further characterization of nuclear changes, we used mouse embryonic fibroblasts (MEF) obtained from *Lmna*$^{H222P/H222P}$ mice. In these cells, nuclei had markedly irregular shape, and in addition small particles with similar electron density to nucleus were seen (Fig. 2A, arrow). In some areas, there was blurring of the nuclear membrane, probably suggesting the disruption of nuclear membrane, where small circular structures were accumulated (Fig. 2A, arrowheads). Vacuolar structures from 3 to 7 μm in diameter were frequently found in the cytoplasm, especially near the blurred nuclear membrane, and appeared to fuse with one another (Fig. 2B). These vacuolar structures were mostly single- or double-membraned although in some cases it was difficult to recognize clear membranous structures (Fig. 2B and C). Smaller electron-dense vesicles were also much increased over the cytoplasm but more highlighted around large vacuolar structures (Fig. 2C and D). The contents of vacuolar structures were variable from granular substances to pieces of amorphous materials, but a few were empty (Fig. 2E–H).

Nuclear shape of cultured *Lmna*$^{H222P/H222P}$ MEF. To characterize perinuclear vacuolar structures by in vitro analysis, we performed immunocytochemistry on *Lmna*$^{H222P/H222P}$ MEF using antibodies against nuclear envelope proteins (e.g., lamins A, C and B, emerin and LAP2). The nuclei had markedly irregular shape and, in addition, single or multiple blebs and nuclear herniation were seen in 21 ± 1.8% of *Lmna*$^{H222P/H222P}$ cells (Fig. S2), similar to previous reports on fibroblasts from patients with *LMNA* mutations.[32,33] Nuclear envelope proteins were intensely stained at bleb sites (Fig. S2, arrowheads). Moreover, various-sized DAPI positive particles were often identified in the cytoplasm around nuclei

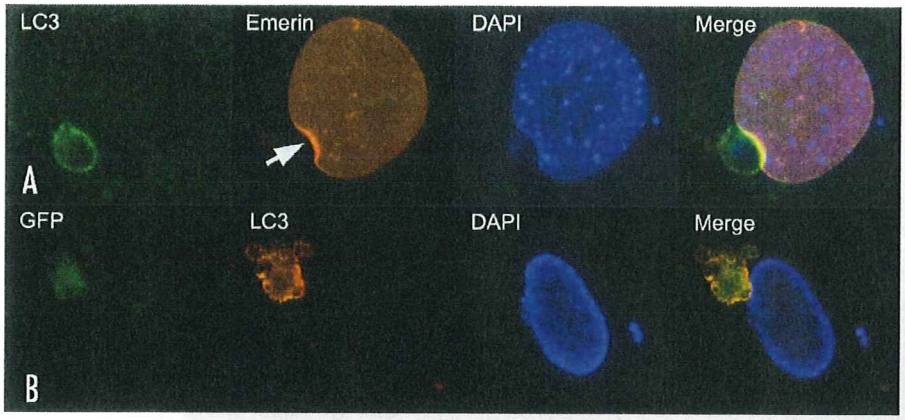

Figure 2. Electron microscopic findings of perinuclear vacuolar structures in *Lmna*$^{H222P/H222P}$ MEF. (A) A particle with similar electron density to the nucleus is detected near the nucleus (arrow). A part of nuclear membrane is blurred suggesting the disruption of nuclear membrane, where small circular structures are present (arrowheads). Vacuolar structures are identified near the nucleus, especially around the ruptured nuclear membrane. (B–D) Some cells contained multiple double- or single-membraned vacuolar structures together with electron dense smaller vesicles. (E–H) The contents of vacuolar structures are variable showing granular substances that fills the whole vacuole, or pieces of amorphous particles. A few are empty. Bars, 0.5 μm.

(Fig. S2, arrows). On the other hand, most of the wild-type cells displayed clearly round shape of nuclei; small blebs were identified only in less than 1% of the cells, and DAPI-positive particles were rarely seen outside nuclei.

Round-shaped LC3-positive signals close to the nuclei in *Lmna*$^{H222P/H222P}$ MEF. As we have insinuated that the vacuolar structures near the nuclei observed under electron microscope could be autophagic in nature, we performed immunocytochemical analysis of microtubule-associated protein 1/light chain 3 (LC3) in *Lmna*$^{H222P/H222P}$ fibroblasts. LC3 is a homologue of yeast Atg8 and is commonly used as a marker of autophagy because it decorates inner and outer membranes of autophagosome.[34] In about 10% of *Lmna*$^{H222P/H222P}$ cells, characteristically round LC3-positive signals were detected near or attached to the nucleus. The part of nuclear membrane interfacing with LC3-staining was sometimes strongly stained with lamins and emerin (Fig. 3A, arrow). Similar findings were also observed in *Lmna*$^{-/-}$ fibroblasts.

Large-sized, round-shaped GFP staining close to nuclei in *Lmna*$^{H222P/H222P}$*/GFP-LC3* MEF. To further characterize the autophagic nature of these perinuclear structures, we produced *Lmna*$^{H222P/H222P}$*/GFP-LC3* transgenic mice. Green fluorescent protein-tagged-LC3 (GFP-LC3) transgenic mouse model has been developed for in vivo analysis of autophagy.[35] On immunocytochemistry, MEF from *Lmna*$^{H222P/H222P}$*/GFP-LC3* mice showed similar frequency of abnormally-shaped nuclei to *Lmna*$^{H222P/H222P}$ cells. In addition, perinuclear round GFP-positive staining, sometimes bigger than the nuclei, were detected in about 10% of observed cells whereas it was rarely seen in wild-type/*GFP-LC3* cells under similar standard culture condition. In addition, these GFP-positive perinuclear signals were almost completely colocalized with LC3 in *Lmna*$^{H222P/H222P}$*/GFP-LC3* cells (Fig. 3B), being diffusely distributed over or outlining GFP signal.

As the activation of autophagy is induced by the upregulation of certain molecules, we examined the expression of other known autophagy-related proteins in *Lmna*$^{H222P/H222P}$*/GFP-LC3* fibroblasts to know whether similar machinery to macroautophagy is working in these cells. In a considerable number of cells, the perinuclear GFP-positive signals colocalized with Atg5 and Atg16L (Fig. 4A), which are known to participate in the initiation of phagophore (or preautophagosome) formation in mammalian cells.[36] Along the border of the perinuclear GFP-positive signals, we observed positive immunoreaction to Atg9 (Fig. 4B), which is associated with phagophore expansion.[37] The GFP signals also colocalized with Rab7 (Fig. 4C), which is known as a small GTPase protein associated with autophagosome maturation.[38] We also checked the involvement of lysosomes, and found that LAMP2, a lysosomal membrane protein, was identified around and inside GFP-positive staining (Fig. 4D); this finding was confirmed by the colocalization of GFP signals with Lyso-Tracker® which marks lysosmes (Fig. 4E). With these findings, we can consider that the large perinuclear GFP signals are giant autophagosomes/autolysosomes.

Intriguingly, GFP-positive autophagosomes/autolysosomes contained extranuclear DAPI with variable staining intensity from intense to blurred or faint (Figs. 3–5). These DAPI signals were colocalized with histone H1 (Fig. 5A), but were rarely co-stained with nuclear envelope proteins such as lamin A and B (Fig. 5B and C), indicating that these are actually extranuclear and may indicate damaged DNA. We therefore immunostained with anti-γH2AX, a marker of DNA double-strand breaks caused by various insults which is known to have certain roles in the recognition and repair of damaged DNA.[39] Some of the extranuclear DAPI signal was colocalized with γH2AX and contained in GFP-positive autophagosomes/autolysosomes (Fig. 5D, arrowhead). γH2AX was detected also in intranuclear portions, mainly in bleb sites (data not shown). These results suggest that extranuclear damaged DNA is destined for autophagic degradation. On the other hand, we could not find any overlap staining of LC3 and DAPI in rarely observed markedly fragmented nuclei with γH2AX staining, although LC3 positive signals can be seen in the cytoplasm (Fig. 5E).

Notably, in wild-type/*GFP-LC3* cells, similar autophagosomes/autolysosomes containing extranuclear DAPI signals were likewise observed, but with rare frequency of less than 0.1%.

Both LC3-II protein amount and transcriptional level of Maplc3b were increased in *Lmna*$^{H222P/H222P}$ MEF. On immunoblotting analysis, the protein amount of LC3-II, which is a lipidated form of LC3 and a marker of autophagosome formation, was significantly increased in *Lmna*$^{H222P/H222P}$ compared

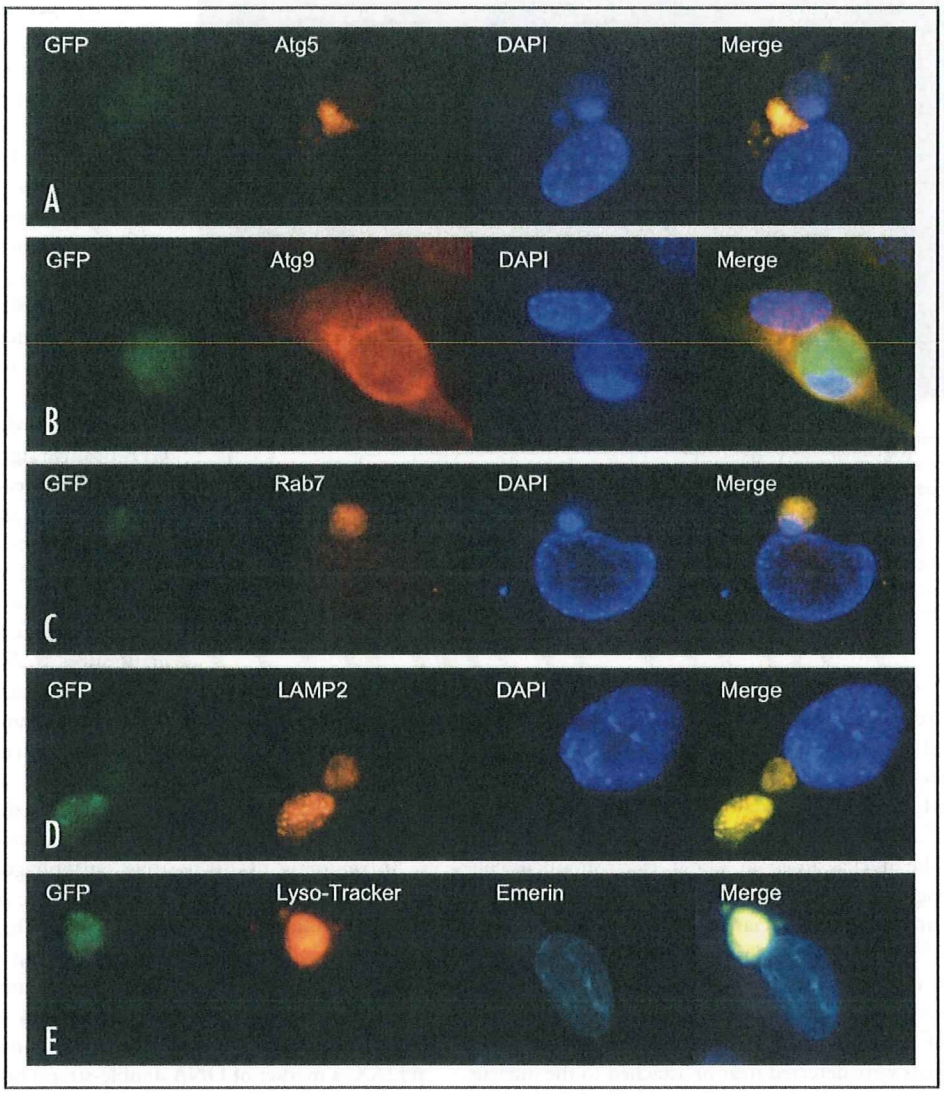

Figure 3. Perinuclear LC3 staining in *Lmna*$^{H222P/H222P}$ and *Lmna*$^{H222P/H222P}$/*GFP-LC3* MEFs. (A) In *Lmna*$^{H222P/H222P}$ MEF, a large-sized and round-shaped LC3-positive vacuolar structure is seen with stronger marginal dot-like staining. DAPI-positive materials are included within. Emerin is more strongly stained in the part of nuclear membrane interfacing with the LC3-positive structures (arrow). (B) In *Lmna*$^{H222P/H222P}$/*GFP-LC3* MEF, LC3 signal is detected with the GFP.

with wild-type cells (Fig. 6A). Because an increased amount of LC3-II could be interpreted either as increased autophagy influx or blocked autophagosome maturation,[40] we quantified the amount of LC3-II with or without lysosomal protease inhibitors (pepstatin A and E64d). LC3-II in *Lmna*$^{H222P/H222P}$ cells was much increased with lysosomal inhibitors (Fig. 6A), implying that the increased LC3-II amount is due to enhanced autophagy influx and not due to impedance of autophagosome maturation.

This increase in LC3-II protein might be also due to transcriptional upregulation of *Maplc3b* encoding a major form of LC3. By quantitative real-time PCR of *Maplc3b*, we observed that the transcriptional level of LC3 was significantly higher in *Lmna*$^{H222P/H222P}$ compared with wild-type MEF (Fig. 6B, $p = 0.0141$); relative copy number of LC3 mRNA in *Lmna*$^{H222P/H222P}$ MEF was 1.36 times when standardized by G3PDH transcriptional level.

Inhibition of autophagy increased the frequency of nuclear abnormalities and decreased cell viability in *Lmna*$^{H222P/H222P}$ MEF. To elucidate the role of autophagy in *Lmna*$^{H222P/H222P}$ cells, we inhibited autophagy by using 3-methyladenine (3-MA) and wortmannin. Autophagy was efficiently inhibited as the amount of LC3-II was notably decreased both in wild-type and *Lmna*$^{H222P/H222P}$ cells (Fig. 7A).

The number of LC3-positive autophagosomes was significantly decreased in the treated *Lmna*$^{H222P/H222P}$ cells compared with the untreated cells (Fig. 7B, $p < 0.0001$). Moreover, LC3 staining was

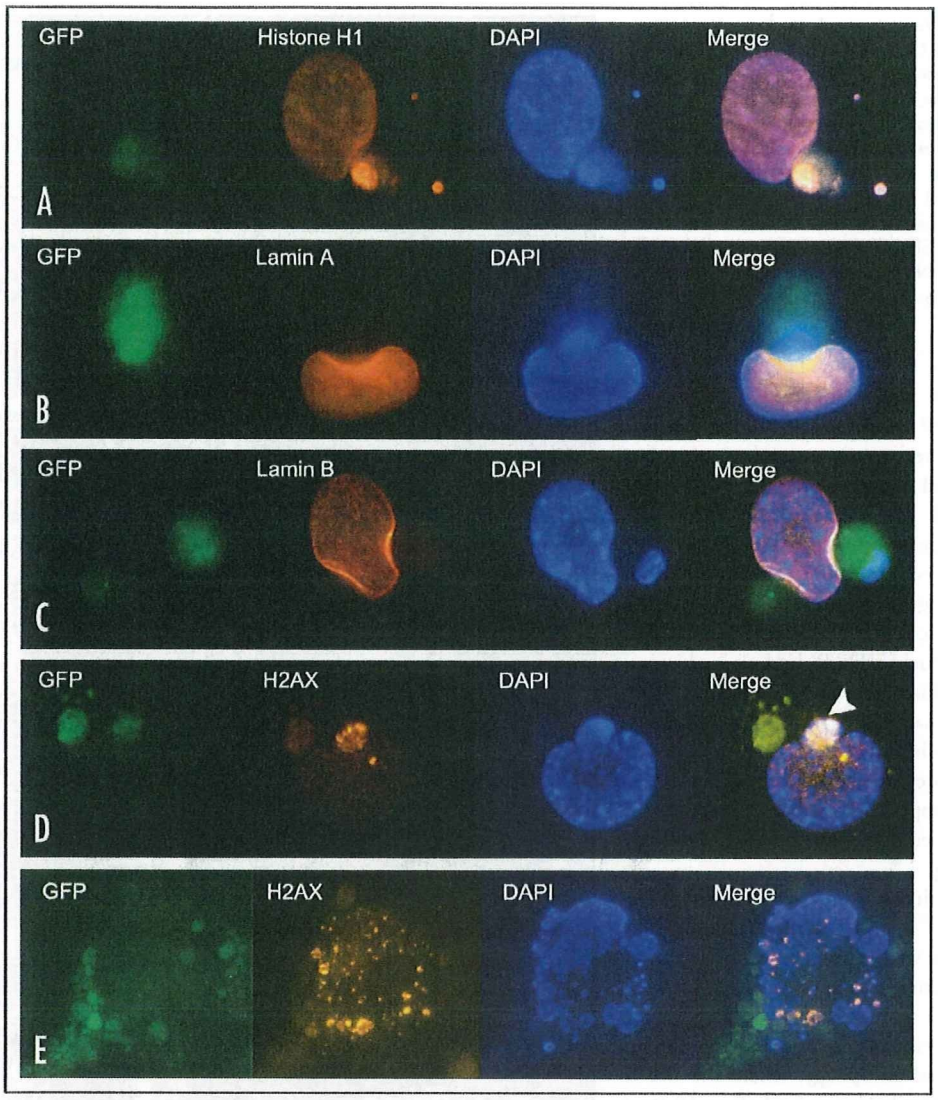

Figure 4. Involvement of autophagy-related proteins and LAMP2, and Lyso-Tracker® probe staining in *Lmna*$^{H222P/H222P}$/*GFP-LC3* MEF. Atg5 (A), Atg9 (B), Rab7 (C) and LAMP2 (D) are all remarkably stained in/around the GFP-positive structures. (E) Lyso-Tracker® is highlighted and localized with the GFP-positive structures near nucleus.

virtually absent in the treated cells, even in nuclei with markedly irregular shape and with extranuclear DAPI signals, whereas it was often presented in untreated cells (Fig. 7C, upper). In addition, the number of cells with markedly irregular nuclei and/or extranuclear DAPI, as represented in Figure 7C, was much increased when autophagy was inhibited: the percentage of cells with nuclear deformation was 6.7 ± 1.2 and 9.8 ± 1.6 (mean ± SD), and cells with single or multiple extranuclear DAPI was 8.3 ± 0.9 and 14.9 ± 1.5 in untreated and treated cells, respectively (Fig. 7D). The difference between the two groups was statistically significant ($p = 0.0008$) after treatment.

We also checked mean survival rate by staining viable and dead cells in untreated wild-type (0.88), treated wild-type (0.83), untreated *Lmna*$^{H222P/H222P}$ (0.87) and treated *Lmna*$^{H222P/H222P}$ (0.72) cells (Fig. 7E). When autophagy was inhibited, the survival rate of *Lmna*$^{H222P/H222P}$ cells was significant decreased ($p = 0.0029$) as compared to wild-type cells. This result implies that autophagy could have a beneficial effect on cell survival.

Discussion

Here we provide evidence that a part of the nucleus is degraded by autophagy when nuclei are damaged and/or partially extruded into the cytoplasm as frequently observed in nuclear envelopathy.

In *Lmna*$^{H222P/H222P}$/*GFP-LC3* MEF, GFP-positive signals were presented near nuclei, which were proved to be identical to LC3-positive autophagosomes. The difference in staining

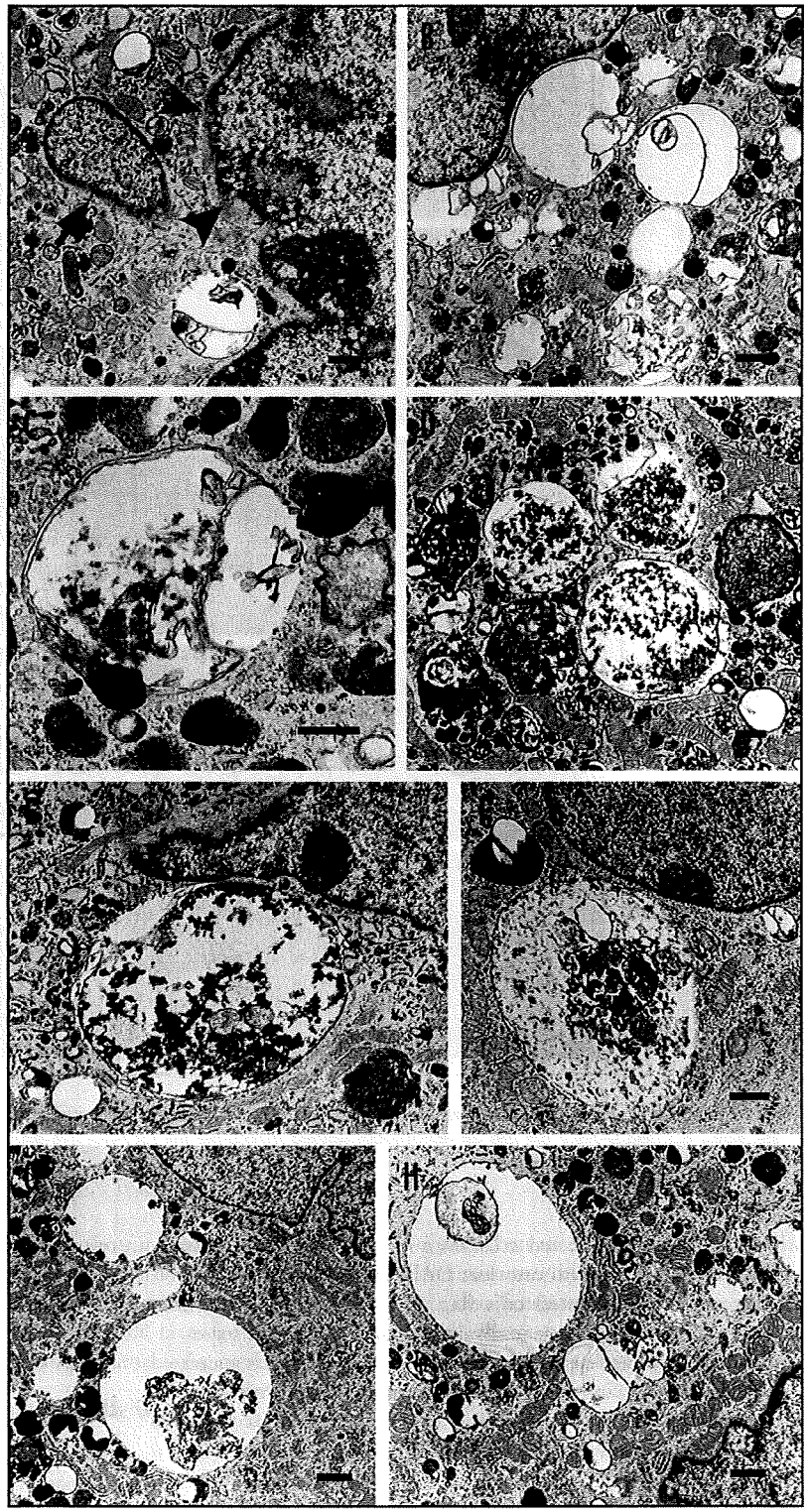

Figure 5. Characterization of nuclear components contained in the GFP-positive autophagosomes on immunocytochemistry. (A–C) GFP-positive autophagosomes with variable sized are seen close to the nuclei, and most of which are partially colocalized with DAPI signals outside of nucleus. Extranuclear DAPI signals in the GFP-positive autophagosomes are positive for histone H1 (A), but not for nuclear envelope proteins such as lamin A and B (B and C). (D) Extranuclear DAPI signals with GFP staining are positive for γH2AX (arrowhead). (E) Nuclear fragments with scattered γH2AX staining are negative for LC3.

pattern between GFP and LC3 despite their essential identity is probably due to the accumulation of GFP that is resistant to lysosomal hydrolase. Further immunostaining of other autophagy-related proteins (i.e., Atg5, 16L, 9 and Rab7) and LAMP2 confirmed that the GFP-positive signals are ultimately autophagosomes and autolysosomes. Our findings indicate that the autophagosomes appear to degrade the extruded nuclear components since most of them contained extranuclear DAPI and major histone protein H1 within. Irregularly blurred or faint DAPI or H1 signals inside the autophagosomes/autolysosomes substantiate that nuclear components are being degraded by autophagic process. The target of autophagy is probably the damaged portions of nuclei as demonstrated by γH2AX immunostaining.

Electron microscopic observations of $Lmna^{H222P/H222P}$ cells demonstrated that autophagosomes were clustered and lysosomes fused to form giant autophagosomes, which were sometimes bigger than nuclei. Giant autophagosomes are quite unusual and are rarely seen in starvation-induced autophagy, where the size is about 1 μm.[35] Similar large-sized (5 to 10 μm) autophagosomes has been reported to encircle bacteria in HeLa cells under group A streptococcus infection although the mechanism to form such giant autophagosomes was not clarified.[41] From our findings it can be suggested that the formation of giant autophagosomes may be required for the degradation of large molecules, such as a part of nucleus.

We propose that $Lmna^{H222P/H222P}$ nuclei, having incomplete lamina structure and frequently subjected to mechanical stress, subsequently become damaged and would apparently require (giant) autophagosome for degradation by lysosomal enzymes. Thus, it seems that this nuclear autophagy is consistent with macroautophagy in terms of its morphology and machinery used. On the other hand, piecemeal microautophagy of nucleus (PMN) has been recently

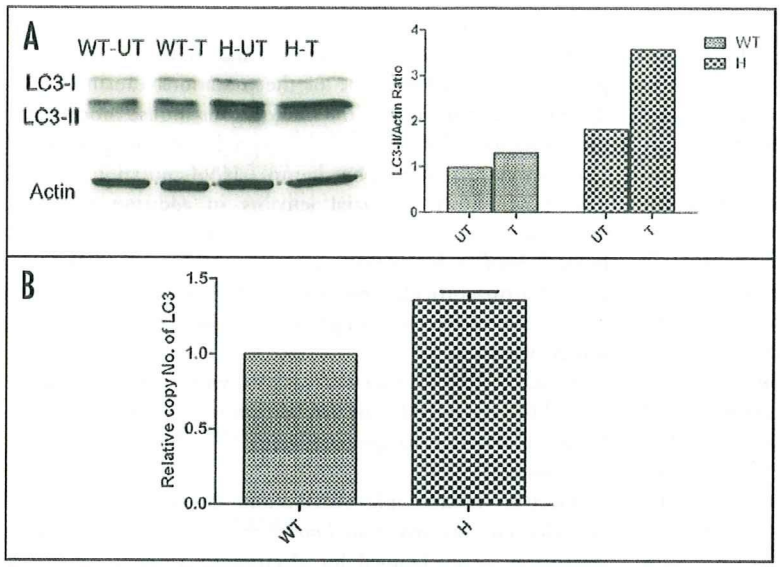

Figure 6. Immunoblotting analysis of LC3 and quantitative real-time PCR of *Maplc3b*. (A) The amount of LC3-II is highly increased in *Lmna*$^{H222P/H222P}$ cells, and which gets more increased with the treatment of lysosomal protease inhibitors (pepstatin A and E64d), suggesting that autophagy is markedly activated in the diseased cells. (B) By quantitative real-time PCR of *Maplc3b*, the transcriptional level of LC3 is represented to be significantly increased in *Lmna*$^{H222P/H222P}$ MEF compared with wild-type ($p = 0.0141$). WT-UT, untreated wild-type; WT-T, treated wild-type; H-UT, untreated *Lmna*$^{H222P/H222P}$; H-T, treated *Lmna*$^{H222P/H222P}$ cells.

reported in *S. cerevisiae*, which is induced by nutritional depletion or rapamycin stimulation. During PMN velcro-like patches are formed by the interaction between vacuolar membrane and outer nuclear membrane at nonessential portions of nuclei.[42] PMN is morphologically categorized as microautophagy because nuclear components are directly engulfed by vacuoles without formation of vesicular intermediates, i.e., autophagosome.[43,44] This concept was further supported by a recent investigation that elucidated the core machinery on PMN.[44] Because detailed underlying molecular mechanism is still unclear, we could not completely exclude the possible involvement of microautophagy for degradation of nuclear blebs observed in *Lmna*$^{H222P/H222P}$ cells.

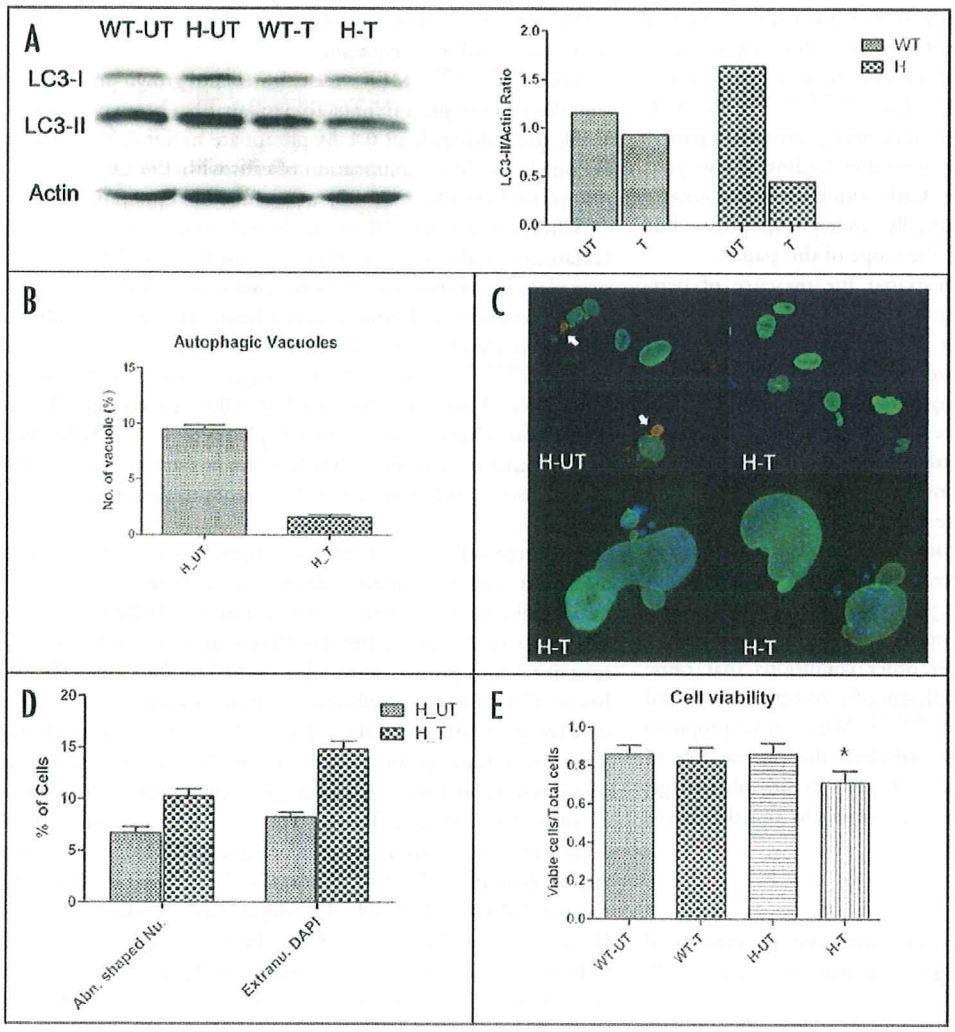

Figure 7. Changes in nuclear abnormalities and cell survival rate after autophagy inhibition. (A) Immunoblotting analysis of LC3 shows that LC3-II is decreased after autophagy inhibition in wild-type and *Lmna*$^{H222P/H222P}$ cells. (B) In treated *Lmna*$^{H222P/H222P}$ cells, autophagic vacuoles are significantly decreased compared with untreated cells ($p < 0.0001$). (C) On immunocytochemistry of LC3 (red), lamin C (green) and DAPI (blue), the treated *Lmna*$^{H222P/H222P}$ cells rarely show LC3 staining whereas untreated cells frequently display perinuclear autophagosomes (arrows, upper). With autophagy inhibition, cells present severe deformation of nuclei and multiple extranuclear DAPI (lower). (D) The number of cells with markedly irregular shaped nuclei and extranuclear DAPI is much increased by autophagy inhibition ($p = 0.0008$) (E) Cell viability assay represents the decreased cell survival rate in *Lmna*$^{H222P/H222P}$ cells by autophagy inhibition compared with wild-type cells (*$p = 0.0029$). WT, wild-type; H, *Lmna*$^{H222P/H222P}$; UT, untreated; T, treated.

The activation of autophagy in $Lmna^{H222P/H222P}$ cells is supported by the finding of increased amount of LC3-II on immunoblotting analysis, and the transcriptional upregulation of LC3 expression. LC3 has been previously reported to be increased in progeroid mice lacking zinc metalloproteinase STE24 or ZMPSTE24 ($Zmpste24^{-/-}$),[45] an enzyme required for the maturation of lamin A. ZMPSTE24 deficiency causes accumulation of the premature form of lamin A (prelamin A) in nuclear envelope and leads to profound nuclear architecture abnormalities.[46] Increased LC3 was thought to be secondary to enhanced basal autophagy in skeletal and cardiac muscles due to a metabolic derangement in progeroid mice. Considering similar molecular defects of nuclear lamina in two mouse models of $Zmpste24^{-/-}$ and $Lmna^{H222P/H222P}$, we cannot totally exclude the possibility of increased basal autophagy in $Lmna^{H222P/H222P}$ mice although they did not show comparable alterations in glucose and lipid metabolism.[47] In this study, the finding that GFP-LC3-positive vacuoles were consistently related to the cytoplasmic nuclear components could indicate that activated autophagy in $Lmna^{H222P/H222P}$ cells may at least in part be induced by the nuclear damage.

Reduced cell viability in $Lmna^{H222P/H222P}$ cells after autophagy inhibition probably resulted from increased frequency of nuclear abnormalities as shown in Figure 7. This result ultimately indicates that autophagy is working for the maintenance of cellular homeostasis by cleaning up nuclear wastes in $Lmna^{H222P/H222P}$ cells. With autophagic degradation of nuclear components, however, a partial loss of genetic information may be inevitable, leading to a varying degree of molecular defects on cells. Cells with bulk loss of genetic materials can be thought to eventually undergo apoptosis, but clarification of this issue is beyond the scope of this paper.

In conclusion, we have demonstrated the presence of perinuclear autophagosomes/autolysosomes in $Lmna^{H222P/H222P}$ cells. Notably, in the area of nuclear membrane interfacing with autophagosomes/autolysosomes, we could see accumulation of nuclear envelope proteins. This may suggest that autophagy could contribute to the rapid repair of the nuclear membrane, as there is a need to rescue the cells from overdegradation or to minimize the loss of nuclear components after nuclear membrane injury. This would be worth exploring in future experiments.

It is also notable that similar autophagosomes/autolysosomes containing nuclear components were found even in wild-type cells although to a much lower frequency. This implies that autophagic degradation of nuclear components is not confined to nuclear envelopathy, and can occur under other conditions that cause nuclear damage. Like other organelle-specific autophagy reported to date, the autophagy in $Lmna^{H222P/H222P}$ MEF can be proposed to be called as 'nucleophagy.' Nevertheless, the precise role of "nucleophagy" in laminopathies, and possibly in physiologic conditions, remains perplexing and a potential interest that needs to be elucidated.

Materials and Methods

Mouse models for nuclear envelopathy and generation of $Lmna^{H222P/H222P}$/GFP-LC3 transgenic mouse. We used H222P homozygous knock-in ($Lmna^{H222P/H222P}$),[47] *Lmna* knockout ($Lmna^{-/-}$),[48] and emerin knockout ($Emd^{-/-}$) mice[25] as mouse models for nuclear envelopathy in this study. The mutation of p.H222P in *LMNA* is one of the mutations causing muscular dystrophy in human, and the homozygous mouse model carrying the mutation, $Lmna^{H222P/H222P}$ reproduced the phenotype of human muscular dystrophy due to *LMNA* mutations.[47] $Lmna^{-/-}$ mice have shown postnatal lethality in addition to muscular dystrophy and cardiomyopathy although they were normal at birth.[48] $Emd^{-/-}$ mice demonstrated altered motor coordination and delayed atrioventricular conduction time in electrocardiogram, but overall they showed normal growth rate and were without obvious muscle weakness.[35]

$Lmna^{H222P/H222P}$ mice were crossed with GFP-LC3 transgenic mice[35] (kindly provided by Dr. Mizushima in Tokyo Medical and Dental University) to generate $Lmna^{H222P/H222P}$/GFP-LC3 transgenic mice.

Electron microscopic observation. Soleus muscles and skin of abdomen obtained from $Lmna^{H222P/H222P}$ mice and wild-type littermates were obtained for electron microscopic observation. Tissues were fixed with 2% glutaraldehyde in 0.1 M cacodylate buffer. After shaking with a mixture of 4% osmium tetroxide, 1.5% lanthanum nitrate and 0.2 M s-collidine for 2 hours, samples were embedded in epoxy resin.

$Lmna^{H222P/H222P}$ MEF were cultured and grown on Lab-Tek™ chambered coverglass (Nunc, Tokyo, Japan). They were fixed with 1.2% glutaraldehyde in 0.1 M phosphate buffer (pH 7.4) at 4°C for one hour. After osmification of cells with 1% OsO4 in 0.1 M phosphate buffer at 4°C, they were embedded in epoxy resin.

Ultrathin sections (50 nm thickness) were stained with uranyl acetate and lead citrate, and then examined under H-600 transmission electron microscope (Hitachi, Japan) at 75 kV.

Cell culture and immunocytochemistry. Mouse embryonic fibroblasts (MEF) were obtained from $Lmna^{H222P/H222P}$, $Lmna^{-/-}$, $Lmna^{H222P/H222P}$/GFP-LC3 transgenic mice and wild-type littermates. They were harvested in 100-mm collagen I-coated dishes with Dulbecco's modified Eagle medium (DMEM, Wako, Osaka, Japan) containing 10% fetal bovine serum (FBS) and 1% of antibiotics, and incubated at 37°C in humidified chamber with 5% CO_2.

Cultured cells were plated on collagen I-coated glass coverslips and fixed with 4% paraformaldehyde in PBS for 15 min at 4°C, permeabilized on ice with 0.25% Triton X-100/PBS for 20 min, blocked with 2% casein/PBS for 15 min at 37°C, and then immunostained with primary antibodies diluted in 2% casein/PBS for 2 hrs at 37°C. Primary antibodies used in this study are as follows: anti-lamin A (Abcam, Tokyo, Japan), lamin C,[16] lamin B (Santa Cruz Biotechnology Inc., CA), emerin (Novocastra Laboratories, Newcastle upon Tyne, UK), lamin-associated protein 2α (LAP2α), nesprin 1α (Abcam, Tokyo, Japan), LC3 (provided by Dr. Ueno, Juntendo university), Atg5 (Sigma-Aldrich, Tokyo, Japan), Atg9 (Biosensis, Thebarton, South Australia), Atg16L, Rab7 (Sigma-Aldrich), LAMP2 (Developmental Studies Hybridoma Bank), histone H1 (Santa Cruz Biotechnology Inc.,), H2AX (Abcam). Cells were then incubated with fluorescently labeled secondary antibodies (Alexa488 or Alexa568) at room temperature